The final publication is available at

https://doi.org/10.1007/s00466-015-1184-8

Additional Information

Anisotropic finite strain viscoelasticity based on the Sidoroff multiplicative decomposition and logarithmic strains

Marcos Latorre · Francisco Javier Montáns

Abstract In this paper a purely phenomenological formulation and finite element numerical implementation for quasi-incompressible transversely isotropic and orthotropic materials is presented. The stored energy is composed of distinct anisotropic equilibrated and nonequilibrated parts. The nonequilibrated strains are obtained from the multiplicative decomposition of the deformation gradient. The procedure can be considered as an extension of the Reese and Govindjee framework to anisotropic materials and reduces to such formulation for isotropic materials.

The stress-point algorithmic implementation is based on an elastic-predictor viscous-corrector algorithm similar to that employed in plasticity. The consistent tangent moduli for the general anisotropic case are also derived. Numerical examples explain the procedure to obtain the material parameters, show the quadratic convergence of the algorithm and usefulness in multiaxial loading. One example also highlights the importance of prescribing a complete set of stress-strain curves in orthotropic materials.

Keywords Viscoelasticity · Hyperelasticity · Logarithmic Strains · Anisotropy · Biological tissues · Polymers

Marcos Latorre
Escuela Técnica Superior de Ingeniera Aeronáutica y del Espacio, Universidad Politécnica de Madrid
Pza.Cardenal Cisneros, 28040-Madrid, Spain
E-mail: m.latorre.ferrus@upm.es

Francisco Javier Montáns (✉)
Escuela Técnica Superior de Ingeniera Aeronáutica y del Espacio, Universidad Politécnica de Madrid
Pza.Cardenal Cisneros, 28040-Madrid, Spain
Tel.: +34 637908304
E-mail: fco.montans@upm.es

1 Introduction

Polymers above the glass transition temperature and biological materials present highly nonlinear hyperelastic (rubbery) behavior coupled with viscous dissipation, see for example [1–5]. Many material models have been proposed for large strain viscoelasticity. Two main approaches may be clearly distinguished [6]: integral-type approaches based on functionals or hereditary integrals which are used to account for the time-dependent and large memory behavior [1, 7–13], see review in [14], and differential-type approaches based on internal state variables frequently motivated on rheological models better suited for short memory behavior, see [15–20] among others. Reference [21] gives a nice overview of both approaches, including stress and strain-like internal variables. Other important contributions are those of Bergström and Boyce [22], Le Tallec et al. [23], Haupt and Sedlan [24] and Lion [25, 26] regarding the internal variables approach. Between both approaches, the latter one is preferred for finite element implementation [2, 16, 18, 27] because the stresses and strains can be computed from the variables at the immediate previous step and there is no need to store a large bulk of information. Furthermore, researchers usually prefer the latter approach because it is easier to obtain the material parameters from experiments [6], in general. However, fractional derivative-type models have also been used to better capture the relaxation procedure employing few material parameters [28], even though the numerical three-dimensional treatment seems to be complex. Integral-type and differential-type approaches can be made equivalent only in some cases, for example in finite linear viscoelasticity [15].

Among internal variable computational approaches, we can distinguish two clearly different types of formu-

lations with important theoretical and numerical implications. The first one was proposed by Simo [15, 27], motivated on a similar small strains framework. This framework has been subsequently used by Holzapfel [16, 19], Kaliske and Rothert [29], Peña et al [17, 18], Liefeith and Kolling [20], Gasser and Forsell [30], among others. The second type of formulation has been proposed by Reese and Govindjee [31]. This formulation is built upon the works of Lubliner [32] who considered a stored energy function consisting on an equilibrated and a nonequilibrated part and the multiplicative decomposition of Sidoroff [33] which is motivated on the similar Lee multiplicative decomposition in elastoplasticity [34, 35].

From a computational standpoint, the formulation of Simo using stress-like internal variables with their respective evolution equations is attractive because it results in a relatively simple numerical algorithm with reduced memory needs thanks to a one-step second-order accurate recurrence formula [15]. This procedure is based on the ideas of Herrmann and Peterson [36] and Taylor et al [37]. However, as noted by Hartmann [38] and Eidel and Kuhn [39], the preservation of second order accuracy is not achieved in general in the finite element context. Furthermore, these type of formulations are only adequate for small deviations from thermodynamical equilibrium because the evolution equations are linear differential equations connected to finite elasticity, whereas the problem is fully nonlinear [14,31,40]. See also [7], Sec. 40, and discussion in [40] regarding a formulation valid for large deviations from equilibrium using this framework.

In essence, the framework from Simo consists on an initial stored energy which may be anisotropic and from which the initial (second Piola–Kirchhoff) stresses are obtained. The internal stresses, whose evolution is given in the form of a linear rate equation typical of the (three parameter) standard solid, subtract from the initial stresses to yield the actual stresses. Then, the actual stresses are not directly derived from a stored energy, although from a theoretical point of view the existence of such potential may be assumed [16]. As noted in [27], the resulting formulation only recovers nonlinear elasticity for instantaneous and equilibrium deformations. For the latter relaxed case, the stored energy is usually set to be a fraction of the initial one given by a material parameter. Furthermore, the procedure is only consistent with the multiplicative decomposition of Sidoroff [33] in some special cases, as when using neo-Hookean stored energies in terms of the right Cauchy–Green metric [27].

The approach followed by Reese and Govindjee [31] is more appealing in the sense that it is fully nonlin-ear, based on the Sidoroff multiplicative decomposition and arguably more adequate (simpler) for situations arbitrarily away from thermodynamic equilibrium. The additive split of the stored energy used in the formulation results in an also additive split of the stress tensor into equilibrated and nonequilibrated addends, a feature which simplifies considerably the formulation. Additive decompositions of energies and hence of stresses have also been used by Holzapfel [16, 19], Pioletti et al [41] and Merodio and Goicolea [42] but in these last two cases including rate effects in the viscous potential which easies the theoretical treatment in terms of some selected invariants. Other similar formulations based on isotropic equilibrated and nonequilibrated contributions are those of Bonet [43], Perić and Dettmer [44] and Nedjar [45] among others.

As mentioned, the model of Reese and Govindjee is also based on the (Sidoroff) multiplicative decomposition of the deformation gradient into a nonequilibrated elastic deformation gradient and a viscous one. The former results in the internal variable used by the model to compute the distinct fully nonlinear nonequilibrated part, a clear difference with Simo's approach. Furthermore, their formulation uses logarithmic stress and strain measures, which result in a more intuitive framework [46] and an attractive computational procedure in which logarithmic strains are updated in an additive way, or alternatively stretches in an exponential form. This is a similar set-up to that used in large strain computational elastoplasticity in which the natural properties of logarithmic strains are exploited, performing volume-preserving inelastic flows and even employing small strains integration algorithms during the plastic correction either for isotropic cases [47, 48] or anisotropic ones [49, 50]. A parallelism with computational elastoplasticity can be established. Many anisotropic constitutive models –see [51, 52], among others– are based on plastic metrics which are interpreted as internal variables and conveniently integrated and updated. A similar additive formulation for viscous (electro-active) polymers can be found in [53]. However, it is possible to develop formulations which do not rely on those metrics but directly on Lee's decomposition and in which the elastic strains are directly computed from the trial state [47–50] as in the small strain case. In a similar fashion the formulation of Reese and Govindjee uses the Sidoroff decomposition to build the nonequilibrated strains which are again computed directly from the trial state.

However, despite of its attractive features, the formulation of Reese and Govindjee is valid only for isotropy [31,54], whereas the framework of Simo is valid for anisotropic stored energies even though the viscous con-

tribution is isotropic [15, 16, 27]. Hence, Simo's framework is still widely used for anisotropic materials [20], particularly for fibre-reinforced materials like many living tissues, see for example [17,18,55]. It is interesting to note that most hyperelastic formulations on anisotropic materials are built upon their constituents, also when using frameworks similar to that of Reese and Govindjee, see for example [56,57]. Whereas this micromechanical approach is interesting in order to understand the physics behind the problem and simplifies the numerical treatment considerably, it is difficult to include all interactions among components or even frequently to accurately measure the behavior of them in an isolated manner as it is the case of living tissues. Moreover, the addition of a viscous component complicates the problem substantially. Hence, a continuum finite viscoelastic formulation which considers the anisotropic material as a whole and is valid for large deviations from thermodynamical equilibrium is needed.

Recently we have presented a novel formulation for isochoric transversely isotropic materials [58] and for isochoric orthotropic materials [59] in which the shape of the stored energy is not given a priori, but directly obtained from experiments by solving the proper equilibrium and compatibility equations. We considered the material as a whole and we have been able to simultaneously and accurately (exactly for practical purposes) predict the material behavior for three (transversely isotropic materials) or six (orthotropic materials) experimental tests. We note that all curves are essential in properly capturing the multiaxial behavior of the material, as it is for the case of the three or six material constants needed to correctly characterize linear transversely isotropic or orthotropic incompressible materials. If properly formulated, these models retain material symmetries congruency not only from an analytical point of view but also from a numerical one [60]. These type of procedures can also be extended to damage mechanics to account for Mullins effects [61].

The purpose of this paper is to present a purely phenomenological, continuum-based visco-hyperelastic model and finite element implementation for anisotropic materials. The formulation is built upon the ideas given in Reese and Govindjee [31], i.e. we use the Sidoroff multiplicative decomposition [33] and an additive split of the stored energy into equilibrated and nonequilibrated parts [32]. The only internal variables are the nonequilibrated logarithmic elastic strains which are obtained from the Sidoroff decomposition. The stored energies may be isotropic, transversely isotropic or orthotropic. The fully nonlinear formulation and finite element implementation takes advantage of the singular properties of the logarithmic strains as the natural

extension of the infinitesimal strains [46]. The use of the Sidoroff decomposition in orthotropy implies that some assumption needs to be taken as for the evolution of the material preferred directions due to viscous flow. A similar situation is found in large strain elastoplasticity formulations [50,62,63]. We assume here that the preferred material directions are not modified by the viscous flow, i.e. the material symmetries are the same in the reference and in the intermediate configurations. In line with this assumption, we suggest that the viscosity tensor is isotropic. For the purely isotropic case, the present formulation recovers that of Reese and Govindjee [31].

In the following sections we first motivate the ideas using small strains and quadratic large strain measures and then develop the formulation and numerical algorithm using logarithmic strains. Finally, some demonstrative examples show some features of the model and the applicability for finite element analysis.

2 Motivation: infinitesimal viscoelasticity

The visco-hyperelasticity model for large deformations presented in the next sections is derived using logarithmic strains. Logarithmic strains naturally extend the well-known physical meaning of the infinitesimal strains, both for axial and shear components [46], to the large strain setting. Then, as a natural consequence, we will show in the next sections that the finite strain viscoelasticity formulation presented in this work is just an extension of the infinitesimal theory introduced in this section.

2.1 Continuum theory

Unidimensional viscoelasticity is satisfactorily motivated from the rheological model represented by the well-known standard solid [15], schematically outlined by a mechanical device consisting of two springs and a dashpot being arranged as in Figure 1, where the small elongations of the springs and the viscous dashpot per unit device-length (i.e. infinitesimal strains) are related through

$$\varepsilon = \varepsilon_e + \varepsilon_v \tag{1}$$

On purely physical grounds, the total strain energy density of this unidimensional solid at a given instant t accounts for the stored elastic energy on both springs and it can be additively split as

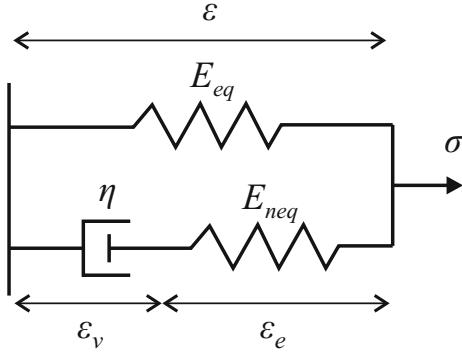$$\Psi(\varepsilon, \varepsilon_e) = \Psi_{eq}(\varepsilon) + \Psi_{neq}(\varepsilon_e) \tag{2}$$

Fig. 1 Standard solid

where Ψ_{eq} and Ψ_{neq} represent the so-called *equilibrated* and *non-equilibrated* strain energy functions associated to the elastic deformations ε and ε_e, respectively. This denomination arises from the fact that $\Psi_{neq}(\varepsilon_e \neq 0) > 0$ accounts for the deviation (in terms of stored energy) from static thermodynamical equilibrium when the total strain ε is fixed. If static equilibrium is attained for that value of ε, then both ε_e and Ψ_{neq} vanish and the resulting strain energy function is $\Psi(\varepsilon, 0) = \Psi_{eq}(\varepsilon)$.

The dissipated power in this rate-dependent system is directly dependent on the rate of ε_v so, even though the natural arguments of the strain energy functions in Eq. (2) are the strain components ε and ε_e, it is convenient to take the total (external) strain ε and the viscous (internal) strain ε_v as the independent variables of the problem. However, note that the non-equilibrated elastic strain ε_e may be also taken as an internal variable with the dependencies $\varepsilon_e(\varepsilon, \varepsilon_v) = \varepsilon - \varepsilon_v$. In rate form, we directly write —we use $\partial(\cdot)/\partial(*)$ to denote partial differentiation, placing also emphasis on the variable which remains fixed in each partial derivative

$$\dot{\varepsilon}_e = \left.\frac{\partial \varepsilon_e}{\partial \varepsilon}\right|_{\dot{\varepsilon}_v = 0} \dot{\varepsilon} + \left.\frac{\partial \varepsilon_e}{\partial \varepsilon_v}\right|_{\dot{\varepsilon} = 0} \dot{\varepsilon}_v = \dot{\varepsilon} - \dot{\varepsilon}_v \quad (3)$$

which, for further use, can be interpreted as the addition of two independent (partial) contributions to $\dot{\varepsilon}_e$

$$\dot{\varepsilon}_e = \left.\dot{\varepsilon}_e\right|_{\dot{\varepsilon}_v = 0} + \left.\dot{\varepsilon}_e\right|_{\dot{\varepsilon} = 0} \quad (4)$$

The rate of the strain energy function in terms of $\dot{\varepsilon}$ and $\dot{\varepsilon}_v$ reads —we use $d(\cdot)/d(*)$ to denote total differentiation

$$\dot{\Psi} = \frac{d\Psi_{eq}}{d\varepsilon} \dot{\varepsilon} + \frac{d\Psi_{neq}}{d\varepsilon_e} \dot{\varepsilon}_e$$

$$= \sigma_{eq} \dot{\varepsilon} + \sigma_{neq}^{|e} \left(\left.\frac{\partial \varepsilon_e}{\partial \varepsilon}\right|_{\dot{\varepsilon}_v = 0} \dot{\varepsilon} + \left.\frac{\partial \varepsilon_e}{\partial \varepsilon_v}\right|_{\dot{\varepsilon} = 0} \dot{\varepsilon}_v \right) \quad (5)$$

with the superscript $(\bullet)^{|e}$ indicating that the variable $(\bullet)$ has been obtained through differentiation with respect to the internal elastic strain ε_e.

The mechanical power dissipated in the device must be non-negative, hence we arrive to the inequality

$$\sigma \dot{\varepsilon} - \dot{\Psi} = \left(\sigma - \sigma_{eq} - \sigma_{neq}^{|e} \left.\frac{\partial \varepsilon_e}{\partial \varepsilon}\right|_{\dot{\varepsilon}_v = 0} \right) \dot{\varepsilon}$$

$$- \sigma_{neq}^{|e} \left.\frac{\partial \varepsilon_e}{\partial \varepsilon_v}\right|_{\dot{\varepsilon} = 0} \dot{\varepsilon}_v \geq 0 \quad (6)$$

In the absence of viscous strain rate, i.e. $\dot{\varepsilon}_v = 0$, the deformation is conservative and the equality must hold, so the total (external) stress in Figure 1 is

$$\sigma = \sigma_{eq} + \sigma_{neq}^{|e} \left.\frac{\partial \varepsilon_e}{\partial \varepsilon}\right|_{\dot{\varepsilon}_v = 0} = \sigma_{eq} + \sigma_{neq} \quad (7)$$

This last expression gives the way in which the non-equilibrated stress σ_{neq} is obtained from the non-equilibrated strain energy function Ψ_{neq}, i.e. taking the partial derivative of $\Psi_{neq}(\varepsilon_e) = \Psi_{neq}(\varepsilon_e(\varepsilon, \varepsilon_v)) = \Psi_{neq}(\varepsilon, \varepsilon_v)$ with respect to ε —note the abuse of notation employed for Ψ_{neq}

$$\sigma_{neq} = \frac{d\Psi_{neq}}{d\varepsilon_e} \left.\frac{\partial \varepsilon_e}{\partial \varepsilon}\right|_{\dot{\varepsilon}_v = 0} = \left.\frac{\partial \Psi_{neq}}{\partial \varepsilon}\right|_{\dot{\varepsilon}_v = 0} \equiv \frac{\partial \Psi_{neq}(\varepsilon, \varepsilon_v)}{\partial \varepsilon} \quad (8)$$

In this particular case, note that $\partial \varepsilon_e / \partial \varepsilon|_{\dot{\varepsilon}_v = 0} = 1$ so

$$\sigma_{neq} = \sigma_{neq}^{|e} \left.\frac{\partial \varepsilon_e}{\partial \varepsilon}\right|_{\dot{\varepsilon}_v = 0} = \sigma_{neq}^{|e} \quad (9)$$

The distinction between taking derivatives with respect to either total strains or elastic strains will be relevant in the finite deformation context, where different configurations will be introduced. Upon the acceptance of Eq. (7), the dissipation inequality reduces to

$$-\sigma_{neq}^{|e} \left.\frac{\partial \varepsilon_e}{\partial \varepsilon_v}\right|_{\dot{\varepsilon} = 0} \dot{\varepsilon}_v = \sigma_{neq}^{|e} \dot{\varepsilon}_v \geq 0 \quad (10)$$

i.e. the mechanical power dissipated by the dashpot must be non-negative. In order to enforce this physical restriction, we previously rewrite it using the interpretation given in Eq. (4), i.e.

$$-\sigma_{neq}^{|e} \left.\frac{\partial \varepsilon_e}{\partial \varepsilon_v}\right|_{\dot{\varepsilon} = 0} \dot{\varepsilon}_v = -\sigma_{neq}^{|e} \left.\dot{\varepsilon}_e\right|_{\dot{\varepsilon} = 0} \geq 0 \quad (11)$$

which is automatically satisfied if we choose the following flow rule

$$-\left.\frac{d\varepsilon_e}{dt}\right|_{\dot{\varepsilon} = 0} =: \frac{1}{\eta} \sigma_{neq}^{|e} = \frac{1}{\eta} \frac{d\Psi_{neq}}{d\varepsilon_e} \quad \Rightarrow \quad \frac{(\sigma_{neq}^{|e})^2}{\eta} \geq 0 \quad (12)$$

where $\eta > 0$ is the so-called dynamic viscosity of the dashpot, which measures the motion resistance via viscous effects (the greater the value of η, the longer the internal *relaxation* process to reach thermodynamic equilibrium for a given Ψ_{neq} and a fixed ε).

Note that Eq. $(12)_1$ is usually written as $\dot{\varepsilon}_v = \sigma_{neq}/\eta$. However, we want here to remark that the subscript $\dot{\varepsilon} = 0$ in the left-hand side of Eq. $(12)_1$ is just indicating that the rate of the *independent* internal variable ε_v can be alternatively seen as (minus) the rate of the *dependent* internal variable $\varepsilon_e(\varepsilon, \varepsilon_v)$ in a hypothetical situation in which the total strain ε remains fixed. Interestingly, this interpretation of the continuum theory will facilitate the numerical integration of that equation by means of an operator split of $\dot{\varepsilon}_e$, as we briefly introduce next (Section 2.2).

For the special case of infinitesimal linear viscoelasticity η is a constant and $\Psi_{neq} = 1/2 E_{neq}\varepsilon_e^2$, so the evolution Equation $(12)_1$ results in

$$-\left.\frac{d\varepsilon_e}{dt}\right|_{\dot{\varepsilon}=0} = \frac{E_{neq}}{\eta}\varepsilon_e = \frac{1}{\tau}\varepsilon_e \qquad (13)$$

where $\tau := \eta/E_{neq}$ is the relaxation time associated to the Maxwell element in Figure 1. Equation (13) is essentially the classical evolution equation for linear viscoelasticity, i.e.

$$\dot{\varepsilon}_v = \frac{1}{\tau}\varepsilon_e = \frac{1}{\tau}\left(\varepsilon - \varepsilon_v\right) \qquad (14)$$

which, note, is expressed in this case in terms of the internal inelastic strain ε_v.

2.2 Incremental theory

The constitutive equation proposal for one-dimensional viscous flow given in Eq. $(12)_1$ is non-linear in terms of ε_e, in general. Since ε_e is a function of ε and ε_v, this *viscous flow rule* can be integrated by means of a two-step, elastic predictor/viscous corrector incremental scheme to give the internal deformation state at $t + \Delta t$ when the state at t is known and the total strain ε at $t + \Delta t$ is given. Within the *elastic predictor* substep there is no viscous dissipation, so $\dot{\varepsilon}_v = 0$ and the trial state at $t + \Delta t$ is

$$^{tr}\varepsilon_v = {}^t_0\varepsilon_v \qquad (15)$$
$$^{tr}\varepsilon_e = {}^{t+\Delta t}_0\varepsilon - {}^{tr}\varepsilon_v = {}^{t+\Delta t}_0\varepsilon - {}^t_0\varepsilon_v \qquad (16)$$

where ${}^t_0(\cdot)$ represents the amount from the reference state to time t and ${}^{tr}(\cdot)$ stands for trial state quantities. Within the *viscous corrector* substep the total strain rate is frozen and the integration of Eq. $(12)_1$ yields

$$\int_t^{t+\Delta t} d\varepsilon|_{\dot{\varepsilon}=0} = -\int_t^{t+\Delta t}\frac{1}{\eta}\frac{d\Psi_{neq}}{d\varepsilon_e}dt \qquad (17)$$

i.e. using a backward-Euler integration

$$^{t+\Delta t}_0\varepsilon_e - {}^{tr}\varepsilon_e \simeq -\Delta t\left(\frac{1}{\eta}\frac{d\Psi_{neq}}{d\varepsilon_e}\right)_{t+\Delta t} \qquad (18)$$

which in general provides a non-linear viscous correction for ${}^{t+\Delta t}_0\varepsilon_e$ in terms of ${}^{tr}\varepsilon_e$ through

$$^{t+\Delta t}_0\varepsilon_e + \Delta t\left(\frac{1}{\eta}\frac{d\Psi_{neq}}{d\varepsilon_e}\right)_{t+\Delta t} = {}^{tr}\varepsilon_e \qquad (19)$$

In the sections below we will discuss how to deal with equations of this type in a finite element procedure. For the special case of infinitesimal linear viscoelasticity, the viscous correction Eq. (19) becomes linear, i.e.

$$\left(1 + \frac{\Delta t}{\tau}\right){}^{t+\Delta t}_0\varepsilon_e = {}^{tr}\varepsilon_e \quad \Rightarrow \quad {}^{t+\Delta t}_0\varepsilon_e = \frac{{}^{tr}\varepsilon_e}{1 + \dfrac{\Delta t}{\tau}} \quad (20)$$

Finally, the linear evolution Equation (14), expressed in terms of the viscous internal variable ε_v, can be analytically integrated with the proper initial condition using the convolution representation [15]. These type of analytical solutions have motivated a remarkably different type of incremental integration algorithms for finite linear viscoelasticity based on stress-like (viscous) internal variables, cf. for example Refs. [15–17, 27, 30].

3 Finite strain viscoelasticity: material and spatial continuum formulations

The preceding one-dimensional viscoelastic model for small strains has been built on the basis of the kinematical assumption of additive elastic ε_e and inelastic ε_v internal strains. Within the context of three-dimensional large deformations, a generalization of this decomposition in terms of some finite deformation measure is needed as point of departure in order to formulate strain-based constitutive viscoelastic models. To this end, following the lines of the Lee decomposition for finite elastoplasticity, the so-called Sidoroff's multiplicative decomposition of the deformation gradient $\boldsymbol{X}$ assumes [33] —note that this tensor is usually written as $\boldsymbol{F}$, but we adopt the notation given in Ref. [64]

$$\boldsymbol{X} = \boldsymbol{X}_e\boldsymbol{X}_v \qquad (21)$$

where $\boldsymbol{X}_v$ includes the *viscous* contribution to the total deformation and $\boldsymbol{X}_e$ accounts for the remaining *elastic* contribution, see Figure 2. Having in mind the standard solid of Figure 1, the intermediate state may be seen as the internal, stress-free configuration obtained by the hypothetical elastic unloading of the *equivalent* Maxwell element from the current configuration
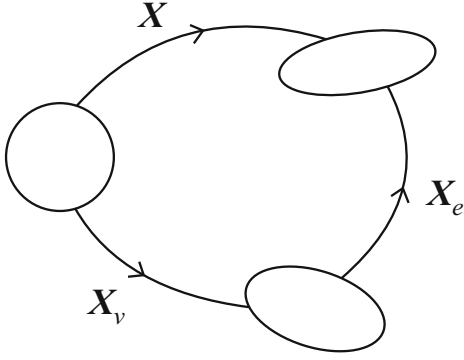
Fig. 2 Sidoroff's multiplicative decomposition of the deformation gradient $\boldsymbol{X} = \boldsymbol{X}_e \boldsymbol{X}_v$.

by means of $\boldsymbol{X}_e^{-1}$ [22]. However, note that the rheological model of Figure 1, based on additive internal strains, does not exactly corresponds to the one-dimensional version of Eq. (21), based on multiplicative internal stretches, i.e. $\lambda = \lambda_e \lambda_v$. Interestingly, the same additive structure shown in Figure 1 is recovered if finite logarithmic strain measures are considered, i.e. $\ln \lambda = \ln \lambda_e + \ln \lambda_v$. Hence, upon the acceptation of the Sidoroff's decomposition hypothesis within the large strain visco-hyperelastic framework, the logarithmic strain measure naturally arises as the large strain measure to be used in constitutive modelling in order to preserve the same algorithmic structure of the small strains formulation. A similar reasoning has led to a variety of finite elastoplasticity formulations based on Lee's decomposition and that preserve the classical return mapping algorithm of the small strain case [47–49, 65].

3.1 Material description

From Eq. (21), the expression of the elastic non-equilibrated right Cauchy–Green tensor $\boldsymbol{C}_e = \boldsymbol{X}_e^T \boldsymbol{X}_e$ in terms of the right Cauchy–Green tensor $\boldsymbol{C} = \boldsymbol{X}^T \boldsymbol{X}$ and the viscous deformation gradient $\boldsymbol{X}_v$ (both $\boldsymbol{C}$ and $\boldsymbol{X}_v$ taken as the independent variables) results in

$$\boldsymbol{C}_e\left(\boldsymbol{C}, \boldsymbol{X}_v\right) = \boldsymbol{X}_v^{-T} \boldsymbol{C} \boldsymbol{X}_v^{-1} = \boldsymbol{X}_v^{-T} \odot \boldsymbol{X}_v^{-T} : \boldsymbol{C} \quad (22)$$

where we have introduced the notation $(\boldsymbol{Y} \odot \boldsymbol{Y})_{ijkl} = Y_{ik}Y_{jl}$ and have omitted symmetrization issues for the matter of notation simplicity. In terms of Green–Lagrange strain measures we have

$$\begin{aligned}\boldsymbol{A}_e\left(\boldsymbol{A}, \boldsymbol{X}_v\right) &= \frac{1}{2}\left(\boldsymbol{C}_e - \boldsymbol{I}\right) = \boldsymbol{X}_v^{-T}\left(\boldsymbol{A} - \boldsymbol{A}_v\right)\boldsymbol{X}_v^{-1} \\ &= \boldsymbol{X}_v^{-T} \odot \boldsymbol{X}_v^{-T} : \left(\boldsymbol{A} - \boldsymbol{A}_v\right)\end{aligned} \quad (23)$$

The material rate of this last equation gives

$$\dot{\boldsymbol{A}}_e = \left.\frac{\partial \boldsymbol{A}_e}{\partial \boldsymbol{A}}\right|_{\dot{\boldsymbol{X}}_v = \boldsymbol{0}} : \dot{\boldsymbol{A}} + \left.\frac{\partial \boldsymbol{A}_e}{\partial \boldsymbol{X}_v}\right|_{\dot{\boldsymbol{A}} = \boldsymbol{0}} : \dot{\boldsymbol{X}}_v \quad (24)$$

Then, analogously to Eq. (4), we identify

$$\dot{\boldsymbol{A}}_e = \left.\dot{\boldsymbol{A}}_e\right|_{\dot{\boldsymbol{X}}_v = \boldsymbol{0}} + \left.\dot{\boldsymbol{A}}_e\right|_{\dot{\boldsymbol{A}} = \boldsymbol{0}} \quad (25)$$

which is a very useful interpretation when one has the total strain energy function expressed in terms of Lagrangian strain tensors. We will take advantage of this fact in the two-step predictor-corrector integration scheme used below. At this point and for further use, we just note that the fourth-order geometrical tensor

$$\left.\frac{\partial \boldsymbol{A}_e}{\partial \boldsymbol{A}}\right|_{\dot{\boldsymbol{X}}_v = \boldsymbol{0}} = \boldsymbol{X}_v^{-T} \odot \boldsymbol{X}_v^{-T} \equiv \frac{\partial \boldsymbol{A}_e(\boldsymbol{A}, \boldsymbol{X}_v)}{\partial \boldsymbol{A}} \quad (26)$$

obtained by direct differentiation in Eq. (23), defines the push-forward and pull-back operations (when the viscous flow is frozen) between $\dot{\boldsymbol{A}}$, defined in the reference configuration, and $\dot{\boldsymbol{A}}_e$, defined in the intermediate configuration. The partial gradient $\partial \boldsymbol{A}_e / \partial \boldsymbol{X}_v$ with $\dot{\boldsymbol{A}} = \boldsymbol{0}$ is easily obtained taking the time derivative of Eq. (22) and identifying terms. However, it is not needed in the formulation we present below.

Motivated by the small strain case, the total stored energy density function is assumed to contain two hyperelastic contributions, an *equilibrated* one associated to the (right) stretch of $\boldsymbol{X}$ and a *non-equilibrated* one associated to the (right) stretch of $\boldsymbol{X}_e$. For example, in terms of Green–Lagrange strains, the stored energy function is

$$\Psi = \Psi_{eq}\left(\boldsymbol{A}\right) + \Psi_{neq}\left(\boldsymbol{A}_e\right) \quad (27)$$

and its material rate —recall the notation introduced in Eq. (5)

$$\begin{aligned}\dot{\Psi} &= \dot{\Psi}_{eq}\left(\boldsymbol{A}\right) + \dot{\Psi}_{neq}\left(\boldsymbol{A}_e\right) \\ &= \frac{d\Psi_{eq}}{d\boldsymbol{A}} : \dot{\boldsymbol{A}} + \frac{d\Psi_{neq}}{d\boldsymbol{A}_e} : \dot{\boldsymbol{A}}_e \\ &= \boldsymbol{S}_{eq} : \dot{\boldsymbol{A}} + \boldsymbol{S}_{neq}^{|e} : \dot{\boldsymbol{A}}_e\end{aligned} \quad (28)$$

where $\boldsymbol{S}$ stand for second Piola–Kirchhoff stresses. The insertion of Eq. (24) into Eq. (28) yields

$$\begin{aligned}\dot{\Psi} &= \left(\boldsymbol{S}_{eq} + \boldsymbol{S}_{neq}^{|e} : \left.\frac{\partial \boldsymbol{A}_e}{\partial \boldsymbol{A}}\right|_{\dot{\boldsymbol{X}}_v = \boldsymbol{0}}\right) : \dot{\boldsymbol{A}} \\ &\quad + \boldsymbol{S}_{neq}^{|e} : \left.\frac{\partial \boldsymbol{A}_e}{\partial \boldsymbol{X}_v}\right|_{\dot{\boldsymbol{A}} = \boldsymbol{0}} : \dot{\boldsymbol{X}}_v\end{aligned} \quad (29)$$

The dissipation inequality in material description

$$\boldsymbol{S} : \dot{\boldsymbol{A}} - \dot{\Psi} = \left(\boldsymbol{S} - \boldsymbol{S}_{eq} - \boldsymbol{S}_{neq}^{|e} : \left. \frac{\partial \boldsymbol{A}_e}{\partial \boldsymbol{A}} \right|_{\dot{\boldsymbol{X}}_v = \boldsymbol{0}} \right) : \dot{\boldsymbol{A}}$$

$$- \boldsymbol{S}_{neq}^{|e} : \left. \frac{\partial \boldsymbol{A}_e}{\partial \boldsymbol{X}_v} \right|_{\dot{\boldsymbol{A}} = \boldsymbol{0}} : \dot{\boldsymbol{X}}_v \geq 0 \qquad (30)$$

is fulfilled if, first ($\dot{\boldsymbol{X}}_v = \boldsymbol{0}$ implies no dissipation, so the equality must hold)

$$\boldsymbol{S} = \boldsymbol{S}_{eq} + \boldsymbol{S}_{neq}^{|e} : \left. \frac{\partial \boldsymbol{A}_e}{\partial \boldsymbol{A}} \right|_{\dot{\boldsymbol{X}}_v = \boldsymbol{0}} = \boldsymbol{S}_{eq} + \boldsymbol{S}_{neq} \qquad (31)$$

and, second, the stresses $\boldsymbol{S}_{neq}^{|e}$ dissipate power when the viscous flow is taking place by means of

$$- \boldsymbol{S}_{neq}^{|e} : \left. \frac{\partial \boldsymbol{A}_e}{\partial \boldsymbol{X}_v} \right|_{\dot{\boldsymbol{A}} = \boldsymbol{0}} : \dot{\boldsymbol{X}}_v \geq 0 \qquad (32)$$

Equation (31) gives the existing geometrical mapping between the non-equilibrated Second Piola–Kirchhoff stress tensors $\boldsymbol{S}_{neq}$, operating in the reference configuration, and $\boldsymbol{S}_{neq}^{|e}$, defined in the relaxed configuration

$$\boldsymbol{S}_{neq} = \boldsymbol{S}_{neq}^{|e} : \boldsymbol{X}_v^{-T} \odot \boldsymbol{X}_v^{-T} = \frac{d\Psi_{neq}}{d\boldsymbol{A}_e} : \left. \frac{\partial \boldsymbol{A}_e}{\partial \boldsymbol{A}} \right|_{\dot{\boldsymbol{X}}_v = \boldsymbol{0}} \qquad (33)$$

which is in correspondence with the mapping given in the first addend of Eq. (24). Hence, note that the mechanical power $\boldsymbol{S}_{neq} : \dot{\boldsymbol{A}}$ is equivalent to the mechanical power $\boldsymbol{S}_{neq}^{|e} : \dot{\boldsymbol{A}}_e$ when the viscous flow is frozen, i.e.

$$\boldsymbol{S}_{neq} : \dot{\boldsymbol{A}} = \boldsymbol{S}_{neq}^{|e} : \left. \dot{\boldsymbol{A}}_e \right|_{\dot{\boldsymbol{X}}_v = \boldsymbol{0}} = \left. \dot{\Psi}_{neq} \right|_{\dot{\boldsymbol{X}}_v = \boldsymbol{0}} \qquad (34)$$

Equation $(33)_2$ provides the following definition for $\boldsymbol{S}_{neq}$ in terms of Ψ_{neq} —again, note the abuse of notation $\Psi_{neq}(\boldsymbol{A}_e) = \Psi_{neq}(\boldsymbol{A}_e(\boldsymbol{A}, \boldsymbol{X}_v)) = \Psi_{neq}(\boldsymbol{A}, \boldsymbol{X}_v)$

$$\boldsymbol{S}_{neq} = \left. \frac{\partial \Psi_{neq}}{\partial \boldsymbol{A}} \right|_{\dot{\boldsymbol{X}}_v = \boldsymbol{0}} \equiv \frac{\partial \Psi_{neq}(\boldsymbol{A}, \boldsymbol{X}_v)}{\partial \boldsymbol{A}} \qquad (35)$$

On the other hand, the dissipation inequality Eq. (32) becomes more familiar if one uses the interpretation given in Eq. (25) —cf. Eq. (11)

$$- \boldsymbol{S}_{neq}^{|e} : \left. \frac{\partial \boldsymbol{A}_e}{\partial \boldsymbol{X}_v} \right|_{\dot{\boldsymbol{A}} = \boldsymbol{0}} : \dot{\boldsymbol{X}}_v = - \boldsymbol{S}_{neq}^{|e} : \left. \dot{\boldsymbol{A}}_e \right|_{\dot{\boldsymbol{A}} = \boldsymbol{0}} \geq 0 \quad (36)$$

i.e.

$$\left. \dot{\Psi}_{neq} \right|_{\dot{\boldsymbol{A}} = \boldsymbol{0}} \leq 0 \qquad (37)$$

which will be very useful in order to define a general anisotropic constitutive equation for the viscous flow in the next Section. At this point, note that Eq. $(36)_2$ is equivalent to the general residual Eq. (14) in Ref. [31] —just differentiate Eq. $(22)_1$ with $\boldsymbol{C}$ constant

$$\left. \dot{\boldsymbol{A}}_e \right|_{\dot{\boldsymbol{A}} = \boldsymbol{0}} = \frac{1}{2} \left. \dot{\boldsymbol{C}}_e \right|_{\dot{\boldsymbol{C}} = \boldsymbol{0}} = - \frac{1}{2} \left(\boldsymbol{l}_v^T \boldsymbol{C}_e + \boldsymbol{C}_e \boldsymbol{l}_v \right) \qquad (38)$$

where $\boldsymbol{l}_v = \dot{\boldsymbol{X}}_v \boldsymbol{X}_v^{-1}$ is the viscous velocity gradient.

3.2 Spatial description

From Eq. (21) one can also obtain the expression of the spatial velocity gradient $\boldsymbol{l} = \dot{\boldsymbol{X}} \boldsymbol{X}^{-1}$ in terms of the elastic velocity gradient $\boldsymbol{l}_e = \dot{\boldsymbol{X}}_e \boldsymbol{X}_e^{-1}$ and the viscous velocity gradient $\boldsymbol{l}_v = \dot{\boldsymbol{X}}_v \boldsymbol{X}_v^{-1}$

$$\boldsymbol{l} = \boldsymbol{l}_e + \boldsymbol{X}_e \boldsymbol{l}_v \boldsymbol{X}_e^{-1} \qquad (39)$$

where $\boldsymbol{l}$ and $\boldsymbol{l}_e$ operate in the current configuration and $\boldsymbol{l}_v$ does in the intermediate configuration. Hence, the elastic deformation rate tensor $\boldsymbol{d}_e = sym(\boldsymbol{l}_e)$ is obtained as a function of the deformation rate tensor $\boldsymbol{d} = sym(\boldsymbol{l})$ and $\boldsymbol{l}_v$ (taken as the independent variables in rate form) through

$$\boldsymbol{d}_e(\boldsymbol{d}, \boldsymbol{l}_v) = \boldsymbol{d} - sym\left(\boldsymbol{X}_e \boldsymbol{l}_v \boldsymbol{X}_e^{-1} \right) \qquad (40)$$

or

$$\boldsymbol{d}_e(\boldsymbol{d}, \boldsymbol{l}_v) = \left. \mathbb{M}_d^{d_e} \right|_{\boldsymbol{l}_v = \boldsymbol{0}} : \boldsymbol{d} + \left. \mathbb{M}_{l_v}^{d_e} \right|_{\boldsymbol{d} = \boldsymbol{0}} : \boldsymbol{l}_v \qquad (41)$$

with the fourth-order mapping tensors $\left. \mathbb{M}_d^{d_e} \right|_{\boldsymbol{l}_v = \boldsymbol{0}}$ and $\left. \mathbb{M}_{l_v}^{d_e} \right|_{\boldsymbol{d} = \boldsymbol{0}}$ playing the role of the partial gradients present in Eq. (24). For further use, we just recognize herein that

$$\left. \mathbb{M}_d^{d_e} \right|_{\boldsymbol{l}_v = \boldsymbol{0}} = \mathbb{I}^S \qquad (42)$$

where $\mathbb{I}^S$ stands for the fourth-order symmetric projector tensor, with components in any given basis

$$\left(\mathbb{I}^S \right)_{ijkl} = \frac{1}{2} \left(\delta_{ik} \delta_{jl} + \delta_{il} \delta_{jk} \right) \qquad (43)$$

Analogously to Eq. (25), we can write Eq. (40) as

$$\boldsymbol{d}_e = \boldsymbol{d}_e(\boldsymbol{d}, \boldsymbol{0}) + \boldsymbol{d}_e(\boldsymbol{0}, \boldsymbol{l}_v) = \left. \boldsymbol{d}_e \right|_{\boldsymbol{l}_v = \boldsymbol{0}} + \left. \boldsymbol{d}_e \right|_{\boldsymbol{d} = \boldsymbol{0}} \qquad (44)$$

Since $\dot{\boldsymbol{A}}_e$ is the pull-back of $\boldsymbol{d}_e$ from the current configuration to the intermediate configuration by means of

$$\dot{\boldsymbol{A}}_e = \boldsymbol{X}_e^T \boldsymbol{d}_e \boldsymbol{X}_e = \boldsymbol{X}_e^T \odot \boldsymbol{X}_e^T : \boldsymbol{d}_e =: \mathbb{M}_{d_e}^{\dot{A}_e} : \boldsymbol{d}_e \qquad (45)$$

note that Eqs. (24) and (44) are just the same expression, but written in different configurations:

$$\dot{\boldsymbol{A}}_e = \mathbb{M}_{d_e}^{\dot{A}_e} : \boldsymbol{d}_e = \mathbb{M}_{d_e}^{\dot{A}_e} : \left. \boldsymbol{d}_e \right|_{\boldsymbol{l}_v = \boldsymbol{0}} + \mathbb{M}_{d_e}^{\dot{A}_e} : \left. \boldsymbol{d}_e \right|_{\boldsymbol{d} = \boldsymbol{0}}$$

$$= \left. \dot{\boldsymbol{A}}_e \right|_{\dot{\boldsymbol{X}}_v = \boldsymbol{0}} + \left. \dot{\boldsymbol{A}}_e \right|_{\dot{\boldsymbol{A}} = \boldsymbol{0}} \qquad (46)$$

This last relation between the additive decompositions of $\dot{\boldsymbol{A}}_e$ and $\boldsymbol{d}_e$ may also be obtained taking the time derivative of Eq. (22) and then identifying the decomposition of Eq. (40). It is instructive to observe in Eq. (46) that the same mapping tensor, i.e. $\mathbb{M}_{d_e}^{\dot{A}_e} = \boldsymbol{X}_e^T \odot \boldsymbol{X}_e^T$, is

employed to relate $\boldsymbol{d}_e$ to $\dot{\boldsymbol{A}}_e$ independently of whether they represent generic rates or are associated to any of the particular cases $\boldsymbol{l}_v = \boldsymbol{0}$ or $\boldsymbol{d} = \boldsymbol{0}$. This consideration will be useful below.

The spatial counterpart of Eq. (28) is

$$
\begin{aligned}
\dot{\Psi} &= \boldsymbol{S}_{eq} : \boldsymbol{X}^T d\boldsymbol{X} + \boldsymbol{S}_{neq}^{|e} : \boldsymbol{X}_e^T \boldsymbol{d}_e \boldsymbol{X}_e \\
&= \boldsymbol{X} \boldsymbol{S}_{eq} \boldsymbol{X}^T : \boldsymbol{d} + \boldsymbol{X}_e \boldsymbol{S}_{neq}^{|e} \boldsymbol{X}_e^T : \boldsymbol{d}_e \\
&= \boldsymbol{\tau}_{eq} : \boldsymbol{d} + \boldsymbol{\tau}_{neq}^{|e} : \boldsymbol{d}_e
\end{aligned} \tag{47}
$$

where we have defined the symmetric Kirchhoff stress tensors $\boldsymbol{\tau}_{eq}$ and $\boldsymbol{\tau}_{neq}^{|e}$ in the current configuration as

$$
\boldsymbol{\tau}_{eq} := \boldsymbol{X} \boldsymbol{S}_{eq} \boldsymbol{X}^T = \boldsymbol{S}_{eq} : \mathbb{M}_d^{\dot{A}} \tag{48}
$$

$$
\boldsymbol{\tau}_{neq}^{|e} := \boldsymbol{X}_e \boldsymbol{S}_{neq}^{|e} \boldsymbol{X}_e^T = \boldsymbol{S}_{neq}^{|e} : \mathbb{M}_{d_e}^{\dot{A}_e} \tag{49}
$$

with $\mathbb{M}_d^{\dot{A}} = \boldsymbol{X}^T \odot \boldsymbol{X}^T$ and $\mathbb{M}_{d_e}^{\dot{A}_e}$ given in Eq. (45). Using Eq. (41), $\dot{\Psi}$ is expressed as

$$
\begin{aligned}
\dot{\Psi} &= \left(\boldsymbol{\tau}_{eq} + \boldsymbol{\tau}_{neq}^{|e} : \mathbb{M}_d^{d_e} \Big|_{\boldsymbol{l}_v = \boldsymbol{0}} \right) : \boldsymbol{d} \\
&\quad + \boldsymbol{\tau}_{neq}^{|e} : \mathbb{M}_{l_v}^{d_e} \Big|_{\boldsymbol{d} = \boldsymbol{0}} : \boldsymbol{l}_v
\end{aligned} \tag{50}
$$

It is straightforward to obtain that the dissipation inequality in spatial description $\boldsymbol{\tau} : \boldsymbol{d} - \dot{\Psi} \geq 0$ is fulfilled if, first

$$
\boldsymbol{\tau} = \boldsymbol{\tau}_{eq} + \boldsymbol{\tau}_{neq}^{|e} : \mathbb{M}_d^{d_e} \Big|_{\boldsymbol{l}_v = \boldsymbol{0}} = \boldsymbol{\tau}_{eq} + \boldsymbol{\tau}_{neq} \tag{51}
$$

and, second, the Kirchhoff stresses $\boldsymbol{\tau}_{neq}^{|e}$ dissipate power with the push-forward of $\boldsymbol{l}_v$ from the intermediate to the current configuration

$$
-\boldsymbol{\tau}_{neq}^{|e} : \mathbb{M}_{l_v}^{d_e} \Big|_{\boldsymbol{d} = \boldsymbol{0}} : \boldsymbol{l}_v = \boldsymbol{\tau}_{neq}^{|e} : \boldsymbol{X}_e \boldsymbol{l}_v \boldsymbol{X}_e^{-1} \geq 0 \tag{52}
$$

where Eq. (40) and the symmetry of $\boldsymbol{\tau}_{neq}^{|e}$ have been used. From Expression (51) for the total Kirchhoff stress tensor $\boldsymbol{\tau}$ we readily identify

$$
\boldsymbol{\tau}_{neq} = \boldsymbol{\tau}_{neq}^{|e} : \mathbb{M}_d^{d_e} \Big|_{\boldsymbol{l}_v = \boldsymbol{0}} = \boldsymbol{\tau}_{neq}^{|e} : \mathbb{I}^S = \boldsymbol{\tau}_{neq}^{|e} \tag{53}
$$

which is an obvious result due to the fact that $\boldsymbol{\tau}_{neq} = \boldsymbol{X} \boldsymbol{S}_{neq} \boldsymbol{X}^T$ and $\boldsymbol{\tau}_{neq}^{|e} = \boldsymbol{X}_e \boldsymbol{S}_{neq}^{|e} \boldsymbol{X}_e^T$ represent the same Kirchhoff stress tensor defined in the current configuration, even though being pushed forward from different configurations —compare to Eqs. (9) and (33)₁. We notice that

$$
\boldsymbol{\tau}_{neq} : \boldsymbol{d} = \boldsymbol{\tau}_{neq}^{|e} : \boldsymbol{d}_e |_{\boldsymbol{l}_v = \boldsymbol{0}} = \dot{\Psi}_{neq} \Big|_{\boldsymbol{l}_v = \boldsymbol{0}} \tag{54}
$$

Finally, the dissipated power due to viscous effects can be rewritten using Eqs. (41) and (44) as

$$
-\boldsymbol{\tau}_{neq}^{|e} : \mathbb{M}_{l_v}^{d_e} \Big|_{\boldsymbol{d} = \boldsymbol{0}} : \boldsymbol{l}_v = -\boldsymbol{\tau}_{neq}^{|e} : \boldsymbol{d}_e |_{\boldsymbol{d} = \boldsymbol{0}} \geq 0 \tag{55}
$$

which can be read as

$$
\dot{\Psi}_{neq} \Big|_{\boldsymbol{d} = \boldsymbol{0}} \leq 0 \tag{56}
$$

Equations (36) and (55) are equivalent in the sense that the fulfillment of one of them implies the fulfillment of the other one. In other words, we are just invoking the equivalence between the material and spatial descriptions of the same (dissipative) mechanical power. Furthermore, it is interesting to note that Eq. (55)₂ gives another interpretation of the general residual Eq. (17) in Ref. [31] –i.e. Eq. (52)₂ above–, which we do not need to further specialize to isotropy.

4 Finite visco-hyperelasticity based on logarithmic stress-strain measures

In Section 3.1 we have taken advantage of the fact that an analytical decomposition in terms of $\boldsymbol{A}$ and $\boldsymbol{X}_v$ is known for the elastic Green–Lagrange strains $\boldsymbol{A}_e$, i.e. Eq. (23). For the reasons discussed above, we are interested in developing a model based on material logarithmic strain measures. The (only apparent) problem that arises herein is that we do not know the general analytical expression $\boldsymbol{E}_e(\boldsymbol{E}, \boldsymbol{X}_v)$, with $\boldsymbol{E}_e = 1/2 \ln \boldsymbol{C}_e$ and $\boldsymbol{E} = 1/2 \ln \boldsymbol{C}$. Hence the partial derivatives tensor $\partial \boldsymbol{E}_e / \partial \boldsymbol{E}$ with the viscous flow frozen is unknown in general —compare to Eq. (26). However, as we show below we can circumvent this issue making use of several known mapping tensors, in this case relating the rate of logarithmic strains to either the rate of Green–Lagrange strains or the corresponding deformation rate tensors.

Following the aforementioned arguments, we propose a strain energy function based on material logarithmic strain measures

$$
\Psi = \Psi_{eq}(\boldsymbol{E}) + \Psi_{neq}(\boldsymbol{E}_e) \tag{57}
$$

The formulation presented in Section 3 is valid for compressible anisotropic viscoelastic materials undergoing large deformations. However, the present work is intended to model the behavior of (nearly-)incompressible viscoelastic materials, for which $J = \det(\boldsymbol{X}) \approx 1$. Hence, in practice, it is convenient to decompose first the deformation gradient using the Flory's decomposition

$$
\boldsymbol{X} = (J^{1/3} \boldsymbol{I}) \boldsymbol{X}^d \tag{58}
$$

where $\det(\boldsymbol{X}^d) = 1$, and, subsequently, decompose the distortional part of the deformation gradient by means of the Sidoroff's decomposition

$$
\boldsymbol{X}^d = \boldsymbol{X}_e^d \boldsymbol{X}_v^d \equiv \boldsymbol{X}_e \boldsymbol{X}_v \tag{59}
$$

Note that with these assumptions at hand, the isochoric nature of the non-equilibrium part is exactly preserved by construction and there is no further need to consider this constraint for the inelastic contribution [21,66,67]. Furthermore, the volumetric external deformation (if any) in Eq. (58) is always at thermodynamic equilibrium, i.e. it may be considered hyperelastic. The usual split of the total strain energy in deviatoric-volumetric uncoupled behaviors is further assumed

$$\Psi = \left[\mathcal{W}_{eq}(\boldsymbol{E}^d) + \mathcal{U}_{eq}(J) \right] + \mathcal{W}_{neq}(\boldsymbol{E}_e^d) \qquad (60)$$

$$= \left[\mathcal{W}_{eq}(\boldsymbol{E}^d) + \mathcal{W}_{neq}(\boldsymbol{E}_e^d) \right] + \mathcal{U}_{eq}(J) = \mathcal{W} + \mathcal{U} \quad (61)$$

where $\mathcal{W} = \mathcal{W}_{eq} + \mathcal{W}_{neq}$ accounts for the contributions to the stored energy Ψ due to the total and elastic deviatoric (true) behaviors, through $\boldsymbol{E}^d$ and $\boldsymbol{E}_e^d$ respectively, and $\mathcal{U} = \mathcal{U}_{eq}$ will be just used herein to impose a volumetric constraint to the deformation in the Finite Element simulations being carried out. Hereafter in this Section, we assume that the three functions present in Eq. $(61)_1$ are known, the former two $\mathcal{W}_{eq}$ and $\mathcal{W}_{neq}$ being determined from experimental data and $\mathcal{U}_{eq}$ being proposed as a proper penalty volumetric function.

The key idea when formulating computational algorithms in finite-element procedures for materials with a history-dependent behavior is to use a recurrence formula involving internal variables that makes possible to compute the internal state at an instant $t + \Delta t$ when the internal state at t is known [15]. Hence, the entire history of strains is not needed and only the internal variables at t are to be stored at the integration points. Particularizing to this case, we need to compute the second Piola–Kirchhoff stress tensor $^{t+\Delta t}\boldsymbol{S}$ derived from the stored energy function given in Eq. (60) and the corresponding tangent moduli $^{t+\Delta t}\mathbb{C}$ when the multiplicative decomposition $^t_0\boldsymbol{X} = {}^t_0 J^{1/3}\, {}^t_0\boldsymbol{X}_e^d\, {}^t_0\boldsymbol{X}_v^d$ is known at t and only the deformation gradient $^{t+\Delta t}_0\boldsymbol{X}$ is known at $t + \Delta t$. To this end, it is convenient to make use of the split given in Eq. (60) into *equilibrated* and *non-equilibrated* parts of Ψ and then simply add both contributions to $^{t+\Delta t}\boldsymbol{S} = {}^{t+\Delta t}\boldsymbol{S}_{eq} + {}^{t+\Delta t}\boldsymbol{S}_{neq}$ and to $^{t+\Delta t}\mathbb{C} = {}^{t+\Delta t}\mathbb{C}_{eq} + {}^{t+\Delta t}\mathbb{C}_{neq}$.

As we will see below, the equilibrated part presents no difficulty because it is readily obtained from the hyperelastic constitutive relation from the total deformation gradient. The more difficult part comes from the non-equilibrated contribution, which needs a viscous constitutive equation and a local iterative procedure in the most general case. We first address the non-equilibrated contribution and then we address the simpler equilibrated one.

5 Non-equilibrated contribution

In order to obtain the purely deviatoric contribution to $\boldsymbol{S}$ and $\mathbb{C}$ at instant $t + \Delta t$ due to Ψ_{neq}, where only the total gradient $\boldsymbol{X}$ is known, it is apparent that we previously need to compute the elastic logarithmic strains $\boldsymbol{E}_e$ at $t + \Delta t$ from the internal variables at t. That is, we need to propose a *viscous flow rule* that gives the evolution of elastic (and viscous) finite strains during the time step Δt. We will see that we can proceed as introduced in Section 2.2 for infinitesimal viscoelasticity, with the only added difficulty being the non-linear kinematic relations involved in the finite deformation context.

5.1 Constitutive equation for the viscous flow

The dissipation inequality in material description given in Eq. $(36)_2$ can be formulated in terms of material logarithmic stress-strain measures through

$$-\boldsymbol{S}_{neq}^{|e} : \dot{\boldsymbol{A}}_e\Big|_{\dot{\boldsymbol{A}}=\boldsymbol{0}} = -\boldsymbol{S}_{neq}^{|e} : \left(\frac{d\boldsymbol{A}_e}{d\boldsymbol{E}_e} : \dot{\boldsymbol{E}}_e\Big|_{\dot{\boldsymbol{E}}=\boldsymbol{0}} \right) \qquad (62)$$

$$= -\left(\boldsymbol{S}_{neq}^{|e} : \frac{d\boldsymbol{A}_e}{d\boldsymbol{E}_e} \right) : \dot{\boldsymbol{E}}_e\Big|_{\dot{\boldsymbol{E}}=\boldsymbol{0}} \qquad (63)$$

$$= -\boldsymbol{T}_{neq}^{|e} : \dot{\boldsymbol{E}}_e\Big|_{\dot{\boldsymbol{E}}=\boldsymbol{0}} \geq 0 \qquad (64)$$

where the elastic-deformation-dependent fourth-order tensor $d\boldsymbol{A}_e/d\boldsymbol{E}_e$ (see Ref. [59]) maps, on the one hand, any material rate $\dot{\boldsymbol{E}}_e$ (in particular $\dot{\boldsymbol{E}}_e\big|_{\dot{\boldsymbol{E}}=\boldsymbol{0}}$, recall Eq. (46)) to its respective material rate $\dot{\boldsymbol{A}}_e$ and, on the other hand (by power conjugacy equivalences), the generalized Kirchhoff stresses $\boldsymbol{T}_{neq}^{|e} := d\Psi_{neq}/d\boldsymbol{E}_e$ to the second Piola–Kirchhoff stresses $\boldsymbol{S}_{neq}^{|e} = d\Psi_{neq}/d\boldsymbol{A}_e$, i.e.

$$\dot{\boldsymbol{A}}_e = \frac{d\boldsymbol{A}_e}{d\boldsymbol{E}_e} : \dot{\boldsymbol{E}}_e , \quad \boldsymbol{T}_{neq}^{|e} = \boldsymbol{S}_{neq}^{|e} : \frac{d\boldsymbol{A}_e}{d\boldsymbol{E}_e} \qquad (65)$$

Due to the fact that $\Psi_{neq}(\boldsymbol{E}_e) = \mathcal{W}_{neq}(\boldsymbol{E}_e^d)$, we note that the non-equilibrated stress tensor $\boldsymbol{T}_{neq}^{|e}$ present in Eq. (64) is purely deviatoric, i.e. traceless:

$$\boldsymbol{T}_{neq}^{|e} = \frac{d\mathcal{W}_{neq}}{d\boldsymbol{E}_e} = \frac{d\mathcal{W}_{neq}}{d\boldsymbol{E}_e^d} : \frac{d\boldsymbol{E}_e^d}{d\boldsymbol{E}_e} = \frac{d\mathcal{W}_{neq}}{d\boldsymbol{E}_e^d} : \mathbb{P}^S \qquad (66)$$

where $\mathbb{P}^S = d\boldsymbol{E}_e^d/d\boldsymbol{E}_e = \mathbb{I}^S - \frac{1}{3}\boldsymbol{I} \otimes \boldsymbol{I}$ is the fourth-order deviatoric projector tensor, with components in any given basis

$$\left(\mathbb{P}^S \right)_{ijkl} = \frac{1}{2} \left(\delta_{ik}\delta_{jl} + \delta_{il}\delta_{jk} \right) - \frac{1}{3}\delta_{ij}\delta_{kl} \qquad (67)$$

Equation (64) can be satisfied enforcing the following *viscous flow rule* —cf. Eq. $(12)_1$

$$-\frac{d\boldsymbol{E}_e}{dt}\Big|_{\dot{\boldsymbol{E}}=\boldsymbol{0}} = \mathbb{V}^{-1} : \boldsymbol{T}_{neq}^{|e} \qquad (68)$$

for a given fourth-order positive-definite viscosity tensor $\mathbb{V}^{-1}$, thereby Eq. (64)

$$\boldsymbol{T}_{neq}^{|e} : \mathbb{V}^{-1} : \boldsymbol{T}_{neq}^{|e} \geq 0 \qquad (69)$$

is automatically fulfilled.

Interestingly, a similar interpretation to that considered in Eq. (68) may be inferred from the non-linear spatial evolution Eq. (21) in Ref. [31]. Consider the non-equilibrated elastic left Cauchy–Green deformation tensor $\boldsymbol{B}_e = \boldsymbol{X}_e \boldsymbol{X}_e^T$ with the dependencies $\boldsymbol{B}_e(\boldsymbol{X}, \boldsymbol{C}_v^{-1}) = \boldsymbol{X} \boldsymbol{C}_v^{-1} \boldsymbol{X}^T$. Then, the Lie derivative of $\boldsymbol{B}_e$ may be alternatively seen as indicated in Eq. $(70)_2$

$$\mathcal{L}\boldsymbol{B}_e = \boldsymbol{X}\frac{d\boldsymbol{C}_v^{-1}}{dt}\boldsymbol{X}^T = \frac{d\boldsymbol{B}_e}{dt}\bigg|_{\dot{\boldsymbol{X}}=\boldsymbol{0}} \qquad (70)$$

which allowed Reese and Govindjee to integrate the flow rule performing an operator split of $\dot{\boldsymbol{B}}_e$ and using the exponential mapping. As a result, an incremental evolution equation in terms of principal elastic logarithmic strains, valid for isotropy behavior only, was derived, cf. Eq. (45) in Ref. [31]. Equation (68) allows us to extend these ideas to anisotropic materials using logarithmic strain measures directly.

5.2 Integration of the evolution equation

The constitutive equation in material rate form given in Eq. (68) can be integrated by means of a two-step, elastic predictor/viscous corrector method. Previously, we obtain $\boldsymbol{C}_e = \boldsymbol{X}_v^{-T}\boldsymbol{C}^d\boldsymbol{X}_v^{-1}$ from Eq. (59), with $\boldsymbol{C}^d = \boldsymbol{X}^{dT}\boldsymbol{X}^d$. Hence we observe the dependencies $\boldsymbol{E}_e = \boldsymbol{E}_e(\boldsymbol{E}^d, \boldsymbol{X}_v)$. Within the elastic predictor step there is no viscous dissipation, whereupon Eq. (32) —equivalently, Eq. (55)— yields

$$\dot{\boldsymbol{X}}_v = \boldsymbol{0} \quad \Rightarrow \quad \dot{\boldsymbol{E}}_e = \dot{\boldsymbol{E}}_e\Big|_{\dot{\boldsymbol{X}}_v=\boldsymbol{0}} \qquad (71)$$

and the trial (isochoric) state at time $t + \Delta t$ is given by (see Figure 3)

$$^{tr}\boldsymbol{X}_v = {}_0^t\boldsymbol{X}_v \qquad (72)$$
$$^{tr}\boldsymbol{X}_e = {}_0^{t+\Delta t}\boldsymbol{X}^d\,{}^{tr}\boldsymbol{X}_v^{-1} = {}_0^{t+\Delta t}\boldsymbol{X}^d\,{}_0^t\boldsymbol{X}_e \qquad (73)$$

where ${}_0^t\boldsymbol{X}_v$ and ${}_0^{t+\Delta t}\boldsymbol{X}^d$ are known. Clearly, the increment of deformation ${}_t^{t+\Delta t}\boldsymbol{X}^d = {}_0^{t+\Delta t}\boldsymbol{X}^d({}_0^t\boldsymbol{X}^d)^{-1}$ is completely applied to the elastic deformation gradient ${}_0^t\boldsymbol{X}_e$ within the trial substep. The trial logarithmic strain tensor is then

$$^{tr}\boldsymbol{E}_e = \frac{1}{2}\ln({}^{tr}\boldsymbol{C}_e) = \frac{1}{2}\ln({}^{tr}\boldsymbol{X}_e^T\,{}^{tr}\boldsymbol{X}_e) \qquad (74)$$

Subsequently, during the viscous corrector substep we enforce —we use $\dot{\boldsymbol{E}} = \boldsymbol{0}$ instead of $\dot{\boldsymbol{E}}^d = \mathbb{P}^S : \dot{\boldsymbol{E}} = \boldsymbol{0}$ for notational simplicity

$$\dot{\boldsymbol{E}} = \boldsymbol{0} \quad \Rightarrow \quad \dot{\boldsymbol{E}}_e = \dot{\boldsymbol{E}}_e\Big|_{\dot{\boldsymbol{E}}=\boldsymbol{0}} \qquad (75)$$

and then we integrate Eq. (68) using a first-order accurate, backward Euler scheme

$$\int_t^{t+\Delta t} d\boldsymbol{E}_e\big|_{\dot{\boldsymbol{E}}=\boldsymbol{0}} = -\int_t^{t+\Delta t} \mathbb{V}^{-1} : \boldsymbol{T}_{neq}^{|e}dt \qquad (76)$$

$$^{t+\Delta t}_{0}\boldsymbol{E}_e - {}^{tr}\boldsymbol{E}_e \approx -\Delta t\left(\mathbb{V}^{-1} : \boldsymbol{T}_{neq}^{|e}\right)_{t+\Delta t} \qquad (77)$$

which provides a non-linear correction for ${}^{t+\Delta t}_{0}\boldsymbol{E}_e$ in terms of ${}^{tr}\boldsymbol{E}_e$ through —compare to Eq. (19)

$$^{t+\Delta t}_{0}\boldsymbol{E}_e + \Delta t\left(\mathbb{V}^{-1} : \frac{d\mathcal{W}_{neq}}{d\boldsymbol{E}_e}\right)_{t+\Delta t} = {}^{tr}\boldsymbol{E}_e \qquad (78)$$

For the most general, non-linear anisotropic case, Eq. (78) is to be solved by means of a local Newton iterative scheme at the quadrature point level of the finite-element procedure (see next Section). Therefore, if $\mathbb{V}^{-1}$ and $\mathcal{W}_{neq}$ are known, we can compute ${}^{t+\Delta t}_{0}\boldsymbol{E}_e$ for a given time step Δt and then proceed to obtain the deviatoric non-equilibrated stresses and tangent moduli at $t + \Delta t$. One important issue that arises herein is due to the fact that $\mathbb{V}^{-1}$ and $\mathcal{W}_{neq}(\boldsymbol{E}_e^d)$ are defined in the intermediate configuration. Hence, for example, if the material is orthotropic, one has to make some assumptions about how the preferred material axes (internally) evolve from the reference to the intermediate configuration. Then, the strain energy function $\mathcal{W}_{neq}$ should be accordingly defined in order to describe the material anisotropy in the relaxed state. One possibility consists of assuming that the preferred material directions transform like material line elements by means of the viscous deformation gradient $\boldsymbol{X}_v$, thereby the reference orthotropic symmetry is lost in the intermediate configuration and the formulation becomes impractical to apply for most problems of interests, so further simplifications are needed, cf. [56]. Other proposed transformations perform a push-forward of the preferred structural tensors such as for velocity gradients, i.e. using the gradient $\boldsymbol{X}_v$ and its inverse, see [68]. As in Ref. [69] in the context of anisotropic viscoelasticity or Ref. [49] for anisotropic elastoplasticity, we will assume herein that the preferred material orientations remain the same in both the intermediate and reference configurations, thus making possible the use of orthotropic spline-based strain energy functions in both configurations [59], i.e. $\mathcal{W}_{eq}(\boldsymbol{E}^d)$ and $\mathcal{W}_{neq}(\boldsymbol{E}_e^d)$. Obviously, any of these important constitutive assumptions
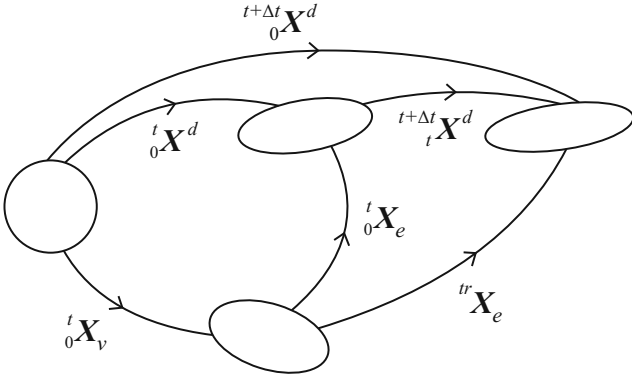
Fig. 3 Multiplicative decomposition of the (isochoric) trial state at $t + \Delta t$. Note $^{tr}\boldsymbol{X}_v = {}_0^t\boldsymbol{X}_v$.

(not experimentally verified) is not needed if the material is assumed isotropic in both the reference and the stress-free configurations, in which case the formulation can be developed in the space of principal strain-stress directions, cf. [31,54].

At this point, only the fourth-order viscosity tensor $\mathbb{V}^{-1}$ remains to be defined. From a mathematical and computational standpoint there would be no problem in using an anisotropic viscous tensor. However, as discussed above, we assume that the viscous flow does not change the (internal) material symmetries during generic deformations. Consistently with this hypothesis, we suggest that the viscous behavior should be isotropic, so there would be no preference in space for the viscous effects. We propose then that $\mathbb{V}^{-1}$ is an isotropic deviatoric tensor, which is expressed in terms of the deviatoric scalar viscosity η^d through

$$\mathbb{V}^{-1} = \frac{1}{2\eta^d} \mathbb{P}^S \qquad (79)$$

In the sections below we will see that the consideration of an isotropic viscosity tensor teamed with equilibrated and non-equilibrated anisotropic hyperelastic functions will result in an anisotropic viscoelastic model in which the relaxation processes associated to the different symmetry directions of the material will be coupled themselves. The evolution equation in rate form, Eq. (68), and its solution in terms of incremental elastic strains, Eq. (78), reduce then to

$$-\left.\frac{d\boldsymbol{E}_e}{dt}\right|_{\dot{\boldsymbol{E}}=\boldsymbol{0}} = \frac{1}{2\eta^d} \frac{d\mathcal{W}_{neq}}{d\boldsymbol{E}_e} \qquad (80)$$

and

$$^{t+\Delta t}_{\quad 0}\boldsymbol{E}_e + \frac{\Delta t}{2\eta^d} \left.\frac{d\mathcal{W}_{neq}}{d\boldsymbol{E}_e}\right|_{t+\Delta t} = {}^{tr}\boldsymbol{E}_e \qquad (81)$$

which, note, are purely deviatoric. For orthotropic materials, $d\mathcal{W}_{neq}/d\boldsymbol{E}_e$ and $\boldsymbol{E}_e$ do not commute. Hence, in

general, $^{t+\Delta t}_{\quad 0}\boldsymbol{E}_e$ and $^{tr}\boldsymbol{E}_e$ in Eq. (81) will not have the same Lagrangian principal basis, which becomes an essential difference between this anisotropic formulation and the isotropic ones. This distinction is similar to that found in anisotropic elastoplasticity [49]. In fact, Eq. (81) may be written as

$$\frac{1}{2}\log\left(^{t+\Delta t}_{\quad 0}\boldsymbol{C}_e\right) = \frac{1}{2}\log\left(^{tr}\boldsymbol{C}_e\right) + \Delta \boldsymbol{E}_e|_{\dot{\boldsymbol{E}}=\boldsymbol{0}} \qquad (82)$$

i.e. for $\Delta t/\eta^d \to 0$

$$^{t+\Delta t}_{\quad 0}\boldsymbol{C}_e \simeq \exp\left(\Delta \boldsymbol{E}_e|_{\dot{\boldsymbol{E}}=\boldsymbol{0}}\right) {}^{tr}\boldsymbol{C}_e \exp\left(\Delta \boldsymbol{E}_e|_{\dot{\boldsymbol{E}}=\boldsymbol{0}}\right) \quad (83)$$

which has a similar format to that of the update in anisotropic elastoplasticity. The difference is that whereas Eq. (83) is an approximation of Eq. (82), in plasticity the situation is reversed. In this case, once a converged solution $^{t+\Delta t}_{\quad 0}\boldsymbol{E}_e$ has been obtained, we update

$$^{t+\Delta t}_{\quad 0}\boldsymbol{X}_e = {}^{tr}\boldsymbol{R}_e {}^{t+\Delta t}_{\quad 0}\boldsymbol{U}_e = {}^{tr}\boldsymbol{R}_e \exp\left(^{t+\Delta t}_{\quad 0}\boldsymbol{E}_e\right) \qquad (84)$$

or

$$\begin{aligned} ^{t+\Delta t}_{\quad 0}\boldsymbol{X}_v &= {}^{t+\Delta t}_{\quad 0}\boldsymbol{X}_e^{-1} {}^{t+\Delta t}_{\quad 0}\boldsymbol{X}^d \\ &= \left(^{t+\Delta t}_{\quad 0}\boldsymbol{U}_e^{-1} {}^{tr}\boldsymbol{U}_e\right) {}_0^t\boldsymbol{X}_v = {}^{t+\Delta t}_{\quad t}\boldsymbol{X}_v {}_0^t\boldsymbol{X}_v \end{aligned} \quad (85)$$

The value of the material parameter η^d in Eq. (81) may be related to, for example, a relaxation time measured from a given experimental test. In order to obtain this relation we linearize the response of the non-equilibrated orthotropic strain energy function $\mathcal{W}_{neq}$ in the flow rule of Eq. (80) to obtain

$$\begin{aligned} -\left.\frac{d\boldsymbol{E}_e}{dt}\right|_{\dot{\boldsymbol{E}}=\boldsymbol{0}} &= \frac{1}{2\eta^d} \left.\frac{d^2\mathcal{W}_{neq}}{d\boldsymbol{E}_e d\boldsymbol{E}_e}\right|_{lin} : \boldsymbol{E}_e \\ &= \mathbb{P}^S : \left(\frac{1}{2\eta^d} \left.\frac{d^2\mathcal{W}_{neq}}{d\boldsymbol{E}_e^d d\boldsymbol{E}_e^d}\right|_{lin}\right) : \mathbb{P}^S : \boldsymbol{E}_e \\ &= \mathbb{P}^S : \left(\sum_i^3 \sum_j^3 \frac{\mu_{ij}^{neq}}{\eta^d} \boldsymbol{L}_{ij}^S \otimes \boldsymbol{L}_{ij}^S\right) : \mathbb{P}^S : \boldsymbol{E}_e \\ &= \mathbb{P}^S : \left(\sum_i^3 \sum_j^3 \frac{1}{\tau_{ij}} \boldsymbol{L}_{ij}^S \otimes \boldsymbol{L}_{ij}^S\right) : \mathbb{P}^S : \boldsymbol{E}_e \end{aligned}$$

$$(86)$$

where

$$\mathcal{W}_{neq}(\boldsymbol{E}_e^d)\big|_{lin} = \sum_i^3 \sum_j^3 \mu_{ij}^{neq} \left.\boldsymbol{E}_e^d\right|_{ij}^2 \qquad (87)$$

is expressed in terms of the orthotropic reference shear moduli μ_{ij}^{neq} and the components of $\boldsymbol{E}_e^d$ in the material orthotropy basis $\{\boldsymbol{a}_1, \boldsymbol{a}_2, \boldsymbol{a}_3\}$ (the subscript lin implies a linearized response, usually at the origin, i.e. quadratic strain energy with constant coefficients). In

the preceding expressions $\boldsymbol{L}_{ij}^{S} = 1/2(\boldsymbol{a}_i \otimes \boldsymbol{a}_j + \boldsymbol{a}_j \otimes \boldsymbol{a}_i)$ stand for the structural tensors associated to the preferred basis. Thus, we obtain

$$\tau_{ij} = \tau_{ji} = \frac{\eta^d}{\mu_{ij}^{neq}} , \quad i, j = \{1, 2, 3\} \tag{88}$$

which represent the orthotropic relaxation times associated to the relaxation processes defined by the components of Eq. (80), see also Eq. (86). Note that we use the same symbol for the relaxation times as for the Kirchhoff stresses but by context confusion is hardly possible. From Eqs. (87) and (88) we observe that the stiffer the non-equilibrated contribution to the material deformation about a given preferred "direction" $\boldsymbol{L}_{ij}^{S}$, the shorter relaxation time associated to that deformation process. We want to remark that with this orthotropic formulation based on an isotropic viscous behavior we can only prescribe one (characteristic) relaxation time obtained from a given relaxation test, for example τ_{mm} from uniaxial testing in the preferred direction $\boldsymbol{a}_m$. In Section 7 we show how to obtain this characteristic relaxation time for orthotropic viscoelasticity. Then, the deviatoric viscosity included in $\mathbb{V}^{-1}$ is

$$\eta^d = \tau_{mm}\mu_{mm}^{neq} = \frac{\tau_{mm}}{2} \left.\frac{\partial^2 \mathcal{W}_{neq}}{(\partial E_{emm}^d)^2}\right|_{lin} \quad \text{(no sum)} \tag{89}$$

and the model predicts relaxation times for the tests in the other directions being weighted by the existing relations between the different deviatoric moduli, i.e.

$$\tau_{pq} = \tau_{mm} \frac{\mu_{mm}^{neq}}{\mu_{pq}^{neq}} \quad \text{(no sum on } m) \tag{90}$$

Once the viscosity parameter η^d has been determined from Eq. (89), the non-linear Equations (80) and (81) are to be used. In those equations we will assume that η^d is deformation independent, which is a usual hypothesis in finite viscoelasticity.

5.3 Local Newton iterations for the non-equilibrated part

Once the trial elastic logarithmic strains ${}^{tr}\boldsymbol{E}_e$ have been obtained using Eq. (74), we proceed to solve Eq. (81) in residual form

$$\boldsymbol{R}(\boldsymbol{E}_e) = \boldsymbol{E}_e + \frac{\Delta t}{2\eta^d} \frac{d\mathcal{W}_{neq}}{d\boldsymbol{E}_e} - {}^{tr}\boldsymbol{E}_e \tag{91}$$

for the most general case when hyperelasticity is non-linear in logarithmic strains. In order to apply Newton's method, take the initial approximation $(k = 0)$

$$\boldsymbol{E}_e^{(k)} = {}^{tr}\boldsymbol{E}_e \tag{92}$$

then evaluate the residual

$$\boldsymbol{R}^{(k)} = \boldsymbol{E}_e^{(k)} + \left.\frac{\Delta t}{2\eta^d} \frac{d\mathcal{W}_{neq}}{d\boldsymbol{E}_e}\right|_{(k)} - {}^{tr}\boldsymbol{E}_e \tag{93}$$

and proceed as usual for every iteration, i.e.

$$\boldsymbol{R}^{(k)} + \left.\frac{d\boldsymbol{R}}{d\boldsymbol{E}_e}\right|_{(k)} : \left(\boldsymbol{E}_e^{(k+1)} - \boldsymbol{E}_e^{(k)}\right) = \boldsymbol{0} \tag{94}$$

Using Eq. (91) we employ

$$\frac{d\boldsymbol{R}(\boldsymbol{E}_e)}{d\boldsymbol{E}_e} = \mathbb{I}^S + \mathbb{P}^S : \frac{\Delta t}{2\eta^d} \frac{d^2 \mathcal{W}_{neq}}{d\boldsymbol{E}_e^d d\boldsymbol{E}_e^d} : \mathbb{P}^S \tag{95}$$

so the update is

$$\boldsymbol{E}_e^{(k+1)} = \boldsymbol{E}_e^{(k)} - \left.\frac{d\boldsymbol{R}}{d\boldsymbol{E}_e}\right|_{(k)}^{-1} : \boldsymbol{R}^{(k)} \tag{96}$$

We perform iterations $(k = 1, 2, ..., m)$ until the norm of the residual tensor $\boldsymbol{R}^{(k)}$ reaches the desired tolerance. Then, at the last iteration, say $k = m$, we can take ${}^{t+\Delta t}_{0}\boldsymbol{E}_e = \boldsymbol{E}_e^{(m)}$. It is apparent that this iterative procedure is volume-preserving.

5.4 Deviatoric contribution to $\boldsymbol{S}$ and $\mathbb{C}$

Once the elastic strains $\boldsymbol{E}_e$ are known at $t + \Delta t$ we can proceed to compute the deviatoric non-equilibrated contribution to the stress and global tangent tensors. First of all, attending to the dependencies $\boldsymbol{A}_e(\boldsymbol{A}^d, \boldsymbol{X}_v)$ (from Eq. (59)) and $\boldsymbol{A}^d(\boldsymbol{A})$ (from Eq. (58)), the non-equilibrated second Piola–Kirchhoff stresses of Eq. (35) result in

$$\begin{aligned}\boldsymbol{S}_{neq} &= \frac{\partial \mathcal{W}_{neq}(\boldsymbol{A}^d, \boldsymbol{X}_v)}{\partial \boldsymbol{A}^d} : \frac{d\boldsymbol{A}^d(\boldsymbol{A})}{d\boldsymbol{A}} \\ &= \left.\frac{\partial \mathcal{W}_{neq}}{\partial \boldsymbol{A}^d}\right|_{\dot{\boldsymbol{X}}_v=\boldsymbol{0}} : \frac{d\boldsymbol{A}^d}{d\boldsymbol{A}} := \boldsymbol{S}_{neq}^{|d} : \frac{d\boldsymbol{A}^d}{d\boldsymbol{A}}\end{aligned} \tag{97}$$

where $d\boldsymbol{A}^d/d\boldsymbol{A}$ represents the fourth-order deviatoric projection tensor in the space of quadratic strains, see Appendix A, and we define the modified second Piola–Kirchhoff stresses $\boldsymbol{S}_{neq}^{|d}$ as the work-conjugate stress measures of $\boldsymbol{A}^d$ such that —recall Eq. (34)

$$\boldsymbol{S}_{neq} : \dot{\boldsymbol{A}} = \boldsymbol{S}_{neq}^{|d} : \dot{\boldsymbol{A}}^d = \left.\dot{\mathcal{W}}_{neq}\right|_{\dot{\boldsymbol{X}}_v=\boldsymbol{0}} \tag{98}$$

However, in order to obtain the non-equilibrated stresses and tangent moduli consistent with the integration algorithm employed, it is convenient to deal with variations of ${}^{tr}\boldsymbol{A}_e$ instead of variations of $\boldsymbol{A}^d$ in Eq. (97). Due to the fact that —note that it is the isochoric counterpart of Eq. (23) specialized to the trial state

$$ {}^{tr}\boldsymbol{A}_e = {}^{tr}\boldsymbol{X}_v^{-T} \odot {}^{tr}\boldsymbol{X}_v^{-T} : \left(\boldsymbol{A}^d - {}^{tr}\boldsymbol{A}_v\right) \tag{99}$$

the rates ${}^{tr}\dot{\boldsymbol{A}}_e$ and $\dot{\boldsymbol{A}}{}^d$ relate to each other through the one-to-one mapping $d\,{}^{tr}\boldsymbol{A}_e/d\boldsymbol{A}^d = {}^{tr}\boldsymbol{X}_v^{-T} \odot {}^{tr}\boldsymbol{X}_v^{-T}$, which remains constant during the finite-element global iterations at time $t+\Delta t$, see Figure 3. Hence, the dependencies of $\boldsymbol{A}_e$ may be re-written as $\boldsymbol{A}_e(\boldsymbol{A}^d\,({}^{tr}\boldsymbol{A}_e)\,,\boldsymbol{X}_v) = \boldsymbol{A}_e\,({}^{tr}\boldsymbol{A}_e,\boldsymbol{X}_v)$ and those of $\mathcal{W}_{neq}$ become $\mathcal{W}_{neq}\,(\boldsymbol{A}_e) = \mathcal{W}_{neq}\,({}^{tr}\boldsymbol{A}_e,\boldsymbol{X}_v)$. The consideration of this change of independent variable in the modified stress tensor present in Eq. (97) yields

$$
\begin{aligned}
\boldsymbol{S}_{neq}^{|d} &= \left.\frac{\partial\mathcal{W}_{neq}}{\partial\boldsymbol{A}^d}\right|_{\dot{\boldsymbol{X}}_v=\mathbf{0}} = \left.\frac{\partial\mathcal{W}_{neq}}{\partial\,{}^{tr}\boldsymbol{A}_e}\right|_{\dot{\boldsymbol{X}}_v=\mathbf{0}} : \frac{d\,{}^{tr}\boldsymbol{A}_e}{d\boldsymbol{A}^d} \\
&= \boldsymbol{S}_{neq}^{|tr} : {}^{tr}\boldsymbol{X}_v^{-T} \odot {}^{tr}\boldsymbol{X}_v^{-T} = {}^{tr}\boldsymbol{X}_v^{-1}\boldsymbol{S}_{neq}^{|tr}\,{}^{tr}\boldsymbol{X}_v^{-T}
\end{aligned}
$$
(100)

where we define the non-equilibrated stresses in the trial intermediate configuration

$$
\boldsymbol{S}_{neq}^{|tr} := \left.\frac{\partial\mathcal{W}_{neq}}{\partial\,{}^{tr}\boldsymbol{A}_e}\right|_{\dot{\boldsymbol{X}}_v=\mathbf{0}} \equiv \frac{\partial\mathcal{W}_{neq}({}^{tr}\boldsymbol{A}_e,\boldsymbol{X}_v)}{\partial\,{}^{tr}\boldsymbol{A}_e}
$$
(101)

as the work-conjugate stresses of ${}^{tr}\boldsymbol{A}_e$, i.e. $\boldsymbol{S}_{neq} : \dot{\boldsymbol{A}} = \boldsymbol{S}_{neq}^{|tr} : {}^{tr}\dot{\boldsymbol{A}}_e$. The modified consistent tangent moduli in the reference configuration $\mathbb{C}_{neq}^{|d}$ relate to the consistent tangent moduli in the trial intermediate configuration $\mathbb{C}_{neq}^{|tr}$ through —note that $d\,{}^{tr}\boldsymbol{A}_e/d\boldsymbol{A}^d$ has only minor symmetries

$$
\begin{aligned}
\mathbb{C}_{neq}^{|d} &= \frac{d\boldsymbol{S}_{neq}^{|d}}{d\boldsymbol{A}^d} = \left(\frac{d\,{}^{tr}\boldsymbol{A}_e}{d\boldsymbol{A}^d}\right)^T : \frac{d\boldsymbol{S}_{neq}^{|tr}}{d\,{}^{tr}\boldsymbol{A}_e} : \frac{d\,{}^{tr}\boldsymbol{A}_e}{d\boldsymbol{A}^d} \\
&= {}^{tr}\boldsymbol{X}_v^{-1} \odot {}^{tr}\boldsymbol{X}_v^{-1} : \mathbb{C}_{neq}^{|tr} : {}^{tr}\boldsymbol{X}_v^{-T} \odot {}^{tr}\boldsymbol{X}_v^{-T}
\end{aligned}
$$
(102)

where the fact that ${}^{tr}\boldsymbol{X}_v^{-T} \odot {}^{tr}\boldsymbol{X}_v^{-T}$ remains constant at each time step has been used. Thus, we are dealt with the task of obtaining the stress and tangent moduli tensors $\boldsymbol{S}_{neq}^{|tr}$ and $\mathbb{C}_{neq}^{|tr}$ in the trial (fixed) intermediate configuration and then just performing the corresponding pull-back operations to the reference configuration (defined by the inverse gradient ${}^{tr}\boldsymbol{X}_v^{-1}$) by means of Eqs. (100) and (102). Subsequently, the deviatoric projection of $\boldsymbol{S}_{neq}^{|d}$ and $\mathbb{C}_{neq}^{|d}$ will give the final non-equilibrated stresses and consistent tangent moduli, cf. Eqs. (114) and (115). We want to emphasize herein that there exists a fundamental difference between the gradient respect to $\boldsymbol{A}^d$ (equivalently, ${}^{tr}\boldsymbol{A}_e$) taken in Eqs. (100) and (102). In Eq. (100), the stresses $\boldsymbol{S}_{neq}^{|d}$ $(\boldsymbol{S}_{neq}^{|tr})$ are obtained through the *partial* gradient of $\mathcal{W}_{neq}$ with respect to $\boldsymbol{A}^d$ $({}^{tr}\boldsymbol{A}_e)$ when the viscous flow at $t+\Delta t$ is frozen, hence the notation $\partial(\cdot)/\partial(*)$ is used and the subscript $\dot{\boldsymbol{X}}_v = \mathbf{0}$ is emphasized. This comes from our theoretical definition of the stresses $\boldsymbol{S}_{neq}$, see Eq. (35), which naturally arises from the dissipation inequality. On the other hand, in Eq. (102) we are interested in

computing the *total* gradient of $\boldsymbol{S}_{neq}^{|d}$ $(\boldsymbol{S}_{neq}^{|tr})$ with respect to $\boldsymbol{A}^d$ $({}^{tr}\boldsymbol{A}_e)$ to be used between consecutive global iterations in the finite element procedure at time step $t+\Delta t$. Since ${}^{t+\Delta t}_0\boldsymbol{X}_v$ does not remain constant at each time step (note that it is implicitly changed by the different viscous corrector substeps), this variation has to be taken into account when computing the gradients given in Eq. (102). Accordingly, the notation $d(\cdot)/d(*)$ is used and the subscript $\dot{\boldsymbol{X}}_v = \mathbf{0}$ is intentionally not indicated in the tangent moduli $\mathbb{C}_{neq}^{|d}$ and $\mathbb{C}_{neq}^{|tr}$ present in that equation. This consideration will lead to the consistent linearization of the integration algorithm employed.

The tensors $\boldsymbol{S}_{neq}^{|tr}$ and $\mathbb{C}_{neq}^{|tr}$ may be obtained from our model, based on logarithmic strains, through

$$
\boldsymbol{S}_{neq}^{|tr} = \left.\frac{\partial\mathcal{W}_{neq}}{\partial\,{}^{tr}\boldsymbol{A}_e}\right|_{\dot{\boldsymbol{X}}_v=\mathbf{0}} = \left.\frac{\partial\mathcal{W}_{neq}}{\partial\,{}^{tr}\boldsymbol{E}_e}\right|_{\dot{\boldsymbol{X}}_v=\mathbf{0}} : \frac{d\,{}^{tr}\boldsymbol{E}_e}{d\,{}^{tr}\boldsymbol{A}_e}
$$
(103)

and —note that the one-to-one mapping $d\,{}^{tr}\boldsymbol{E}_e/d\,{}^{tr}\boldsymbol{A}_e$ has major and minor symmetries

$$
\begin{aligned}
\mathbb{C}_{neq}^{|tr} &= \frac{d\boldsymbol{S}_{neq}^{|tr}}{d\,{}^{tr}\boldsymbol{A}_e} = \frac{d\,{}^{tr}\boldsymbol{E}_e}{d\,{}^{tr}\boldsymbol{A}_e} : \frac{d\boldsymbol{T}_{neq}^{|tr}}{d\,{}^{tr}\boldsymbol{E}_e} : \frac{d\,{}^{tr}\boldsymbol{E}_e}{d\,{}^{tr}\boldsymbol{A}_e} \\
&\quad + \boldsymbol{T}_{neq}^{|tr} : \frac{d^2\,{}^{tr}\boldsymbol{E}_e}{d\,{}^{tr}\boldsymbol{A}_e d\,{}^{tr}\boldsymbol{A}_e}
\end{aligned}
$$
(104)

The generalized Kirchhoff stress tensor in the fixed intermediate configuration

$$
\boldsymbol{T}_{neq}^{|tr} := \left.\frac{\partial\mathcal{W}_{neq}}{\partial\,{}^{tr}\boldsymbol{E}_e}\right|_{\dot{\boldsymbol{X}}_v=\mathbf{0}} \equiv \frac{\partial\mathcal{W}_{neq}({}^{tr}\boldsymbol{E}_e,\boldsymbol{X}_v)}{\partial\,{}^{tr}\boldsymbol{E}_e}
$$
(105)

is to be previously related to the generalized Kirchhoff stress tensor in the updated intermediate configuration $\boldsymbol{T}_{neq}^{|e}$, which is the resulting stress tensor at each global iteration obtained from $\mathcal{W}_{neq}\,(\boldsymbol{E}_e)$ using Eq. (66). Taking into consideration the dependencies $\boldsymbol{E}_e\,({}^{tr}\boldsymbol{E}_e,\boldsymbol{X}_v)$, the application of the chain rule of differentiation gives

$$
\begin{aligned}
\boldsymbol{T}_{neq}^{|tr} &= \left.\frac{\partial\mathcal{W}_{neq}}{\partial\,{}^{tr}\boldsymbol{E}_e}\right|_{\dot{\boldsymbol{X}}_v=\mathbf{0}} = \frac{d\mathcal{W}_{neq}}{d\boldsymbol{E}_e} : \left.\frac{\partial\boldsymbol{E}_e}{\partial\,{}^{tr}\boldsymbol{E}_e}\right|_{\dot{\boldsymbol{X}}_v=\mathbf{0}} \\
&= \boldsymbol{T}_{neq}^{|e} : \left.\frac{\partial\boldsymbol{E}_e}{\partial\,{}^{tr}\boldsymbol{E}_e}\right|_{\dot{\boldsymbol{X}}_v=\mathbf{0}}
\end{aligned}
$$
(106)

Note the analogy between Eq. (106) and Eq. (33) (just change $\boldsymbol{E}_e$ by $\boldsymbol{A}_e$ and ${}^{tr}\boldsymbol{E}_e$ by $\boldsymbol{A}$). Analogously as we did therein, see Eq. (26), the mapping tensor $\partial\boldsymbol{E}_e/\partial\,{}^{tr}\boldsymbol{E}_e$ with the viscous flow frozen is to be obtained taking the corresponding partial derivatives in the analytical expression $\boldsymbol{E}_e\,({}^{tr}\boldsymbol{E}_e,\boldsymbol{X}_v)$. For example, for the simplified cases of isotropic materials under generic deformations or orthotropic materials undergoing finite deformations along the preferred material directions, the trial and updated elastic stretch tensors commute (recall Eq. (81)). Then, from the relation between the trial

and updated (isochoric) states ${}^{tr}\boldsymbol{X}_e\, {}^{tr}\boldsymbol{X}_v = \boldsymbol{X}_e\boldsymbol{X}_v$, and taking ${}^{tr}\boldsymbol{R}_e = \boldsymbol{R}_e$, we readily arrive to —note that only the axial components are relevant and that ${}^{tr}\dot{\boldsymbol{X}}_v = \boldsymbol{0}$ by definition

$$\left.\frac{\partial \boldsymbol{E}_e}{\partial\, {}^{tr}\boldsymbol{E}_e}\right|_{\dot{\boldsymbol{X}}_v=\boldsymbol{0}} = \mathbb{I}^S \quad \Rightarrow \quad \boldsymbol{T}_{neq}^{|tr} = \boldsymbol{T}_{neq}^{|e} \tag{107}$$

For the more general case addressed herein of orthotropic materials undergoing off-axis deformations, the trial and updated elastic material tensors do not commute in general and the analytical expression of $\partial \boldsymbol{E}_e/\partial\, {}^{tr}\boldsymbol{E}_e$ with $\dot{\boldsymbol{X}}_v = \boldsymbol{0}$ is to be computed following another approach (see Appendix B). However, if the time step increment Δt is small with respect to the characteristic relaxation time τ of the orthotropic model at hand, i.e. $\Delta t/\tau \ll 1$, then

$$\left.\frac{\partial \boldsymbol{E}_e}{\partial\, {}^{tr}\boldsymbol{E}_e}\right|_{\dot{\boldsymbol{X}}_v=\boldsymbol{0}} \approx \mathbb{I}^S \quad \Rightarrow \quad \boldsymbol{T}_{neq}^{|tr} \approx \boldsymbol{T}_{neq}^{|e} \tag{108}$$

From now on we will assume that $\boldsymbol{T}_{neq}^{|tr} = \boldsymbol{T}_{neq}^{|e}$ and, as a return, we obtain a much simpler and efficient tangent moduli which are algorithmically consistent with these generalized Kirchhoff stresses. Note that an approximation of this kind is also usual in the context of finite anisotropic elasto-plasticity, see for example Ref. [49], Section 6.4, and note that the assumption $\boldsymbol{S}_{neq}^{|tr} = \boldsymbol{S}_{neq}^{|e}$ (using the nomenclature of this paper) is implicitly considered therein. Then the algorithmic consistent elasto-plastic tangent moduli associated to those stresses is computed in that Reference. If we do not wish to take this approximation, we should compute the analytical mapping tensor present in Eq. (106) and its derivatives in the numerical algorithm, as shown in Appendix B. The modified second Piola–Kirchhoff stresses $\boldsymbol{S}_{neq}^{|d}$ are obtained combining, first, Eqs. (103), (106) and $(107)_1$

$$\boldsymbol{S}_{neq}^{|tr} = \left.\frac{d\mathcal{W}_{neq}}{d\boldsymbol{E}_e}\right|_{t+\Delta t} : \frac{d\, {}^{tr}\boldsymbol{E}_e}{d\, {}^{tr}\boldsymbol{A}_e} \tag{109}$$

and then performing the pull-back to the reference configuration with Eq. (100).

In order to obtain the consistent tangent moduli $d\boldsymbol{T}_{neq}^{|tr}/d\, {}^{tr}\boldsymbol{E}_e$, needed in Eq. (104), we have to take into consideration that the updated logarithmic strain tensor and the trial logarithmic strain tensor relate to each other (when $\dot{\boldsymbol{E}} = \boldsymbol{0}$ and $\dot{\boldsymbol{X}}_v \neq \boldsymbol{0}$) through the one-to-one algorithmic non-linear relation ${}^{t+\Delta t}_0\boldsymbol{E}_e({}^{tr}\boldsymbol{E}_e)$ given in Eq. (81). Hence

$$\frac{d\boldsymbol{T}_{neq}^{|tr}}{d\, {}^{tr}\boldsymbol{E}_e} = \frac{d\boldsymbol{T}_{neq}^{|e}}{d\, {}^{tr}\boldsymbol{E}_e} = \frac{d\boldsymbol{T}_{neq}^{|e}}{d\boldsymbol{E}_e} : \frac{d\, {}^{t+\Delta t}_0\boldsymbol{E}_e}{d\, {}^{tr}\boldsymbol{E}_e} \tag{110}$$

with the tensor $d\, {}^{t+\Delta t}_0\boldsymbol{E}_e/d\, {}^{tr}\boldsymbol{E}_e$ providing the consistent linearization of the algorithmic formulation. Taking derivatives in Eq. (81)

$$\frac{d\, {}^{t+\Delta t}_0\boldsymbol{E}_e}{d\, {}^{tr}\boldsymbol{E}_e} = \left(\mathbb{I}^S + \frac{\Delta t}{2\eta^d}\left.\frac{d^2\mathcal{W}_{neq}}{d\boldsymbol{E}_e d\boldsymbol{E}_e}\right|_{t+\Delta t}\right)^{-1} \tag{111}$$

we obtain the purely deviatoric fourth-order tensor in the trial configuration —note that the volumetric part of Eq. (111) is cancelled in the operation of Eq. (110)

$$\frac{d\boldsymbol{T}_{neq}^{|tr}}{d\, {}^{tr}\boldsymbol{E}_e} = \left.\frac{d^2\mathcal{W}_{neq}}{d\boldsymbol{E}_e d\boldsymbol{E}_e}\right|_{t+\Delta t} : \left.\frac{d\boldsymbol{R}}{d\boldsymbol{E}_e}\right|_{t+\Delta t}^{-1} \tag{112}$$

where the algorithmic gradient $d\, {}^{t+\Delta t}_0\boldsymbol{E}_e/d\, {}^{tr}\boldsymbol{E}_e$ is given by the inverse of Eq. (95) evaluated at the updated strains ${}^{t+\Delta t}_0\boldsymbol{E}_e$, see Section 5.3. It can be shown that the consistent tangent tensor $d\boldsymbol{T}_{neq}^{|tr}/d\, {}^{tr}\boldsymbol{E}_e$, as given in Eq. (112), is symmetric, which is a direct consequence of the fact that the right-hand side of Eq. (68) derives from a Lagrangian creep potential (see Ref. [31] for a formal proof based on an Eulerian creep potential and notice that only the deviatoric contribution is relevant in our formulation). It is again important to emphasize the difference between the gradients given in Eqs. $(107)_1$ (or $(108)_1$) and (111): the former is obtained from a theoretical expression with the viscous flow frozen and is needed to calculate the stresses, whereas the latter is computed from the algorithm when the total deformation gradient is frozen (i.e. during the viscous correction phase) and is needed to calculate the derivatives of the stresses (i.e. consistent tangents). The modified consistent (fully symmetric) tangent moduli $\mathbb{C}_{neq}^{|d}$ for the non-equilibrated part is obtained combining, first, Eqs. (104), $(107)_2$ and (112)

$$\mathbb{C}_{neq}^{|tr} = \frac{d\, {}^{tr}\boldsymbol{E}_e}{d\, {}^{tr}\boldsymbol{A}_e} : \left.\frac{d^2\mathcal{W}_{neq}}{d\boldsymbol{E}_e d\boldsymbol{E}_e}\right|_{t+\Delta t} : \frac{d\, {}^{t+\Delta t}_0\boldsymbol{E}_e}{d\, {}^{tr}\boldsymbol{E}_e} : \frac{d\, {}^{tr}\boldsymbol{E}_e}{d\, {}^{tr}\boldsymbol{A}_e}$$
$$+ \left.\frac{d\mathcal{W}_{neq}}{d\boldsymbol{E}_e}\right|_{t+\Delta t} : \frac{d^2\, {}^{tr}\boldsymbol{E}_e}{d\, {}^{tr}\boldsymbol{A}_e d\, {}^{tr}\boldsymbol{A}_e} \tag{113}$$

and then performing the pull-back to the reference configuration with Eq. (102). All the preceding calculations involving mapping tensors between ${}^{tr}\boldsymbol{A}_e$ and ${}^{tr}\boldsymbol{E}_e$ can be performed in an analogous way, from a numerical perspective, to those corresponding to a typical hyperelastic calculation in terms of total strains $\boldsymbol{A}$ and $\boldsymbol{E}$ (cf. Ref. [59], Section 2.5).

Finally, the corresponding deviatoric projections of $\boldsymbol{S}_{neq}^{|d}$ (Eqs. (100) and (109)) and $\mathbb{C}_{neq}^{|d}$ (Eqs. (102) and (113)) within the space of quadratic strains give the final non-equilibrated stress and consistent tangent moduli tensors as —see Appendix A

$$\boldsymbol{S}_{neq} = \frac{\partial \mathcal{W}_{neq}(\boldsymbol{A}^d, \boldsymbol{X}_v)}{\partial \boldsymbol{A}} = J^{-2/3}\boldsymbol{S}_{neq}^{|d} \tag{114}$$

and

$$\mathbb{C}_{neq} = \frac{d\boldsymbol{S}_{neq}}{d\boldsymbol{A}} = J^{-4/3}\mathbb{C}_{neq}^{|d} \tag{115}$$

As we show in the first example below, the present fully material formulation gives exactly the same results than the spatial formulation in principal directions of Ref. [31] for the particular case of isotropy. Furthermore, the present model provides the formal extension of the model of Ref. [31] to the general anisotropic case, even though the model has been particularized then to the case of material orthotropic symmetry.

5.5 Linearized case: Finite linear viscoelasticity

There are two specific cases in which the constitutive Equation (80) for the viscous flow derived above may be simplified. One of them corresponds to the case in which the hyperelastic constitutive relation between logarithmic stress and strain measures of the non-equilibrated part is linear. For this first case, we just have

$$\mathcal{W}_{neq}(\boldsymbol{E}_e^d) = \sum_i^3 \sum_j^3 \mu_{ij}^{neq} \left. E_e^d \right|_{ij}^2 \equiv \left. \mathcal{W}_{neq}(\boldsymbol{E}_e^d) \right|_{lin} \tag{116}$$

In the second case $\|\boldsymbol{E}_e\| \ll 1$, i.e. only small perturbations $\boldsymbol{E}_e = \boldsymbol{\varepsilon}_e$ away from the thermodynamical equilibrium occur, where $\boldsymbol{\varepsilon}_e$ stands for the infinitesimal strain tensor. In this second case, we can take —note that we are linearizing the non-equilibrated response in the intermediate configuration in this case

$$\mathcal{W}_{neq}(\boldsymbol{\varepsilon}_e^d) = \left. \mathcal{W}_{neq}(\boldsymbol{E}_e^d) \right|_{lin} = \sum_i^3 \sum_j^3 \mu_{ij}^{neq} \left. \varepsilon_e^d \right|_{ij}^2 \tag{117}$$

We show next that both cases lead to the same linear-linearized solution for the evolution equation, i.e. the so-called Finite Linear Viscoelasticity. However, one has to take into account that the former is still valid for finite *elastic* deformations away from the thermodynamic equilibrium (a linear theory in terms of logarithmic strains for large internal strains), whereas the latter is only valid for small non-equilibrated perturbations (a linearized theory for infinitesimal internal strains). Note that the total and viscous gradients $\boldsymbol{X}$ and $\boldsymbol{X}_v$ may represent large deformations in both cases. Since $\boldsymbol{E}_e = \boldsymbol{\varepsilon}_e$ within the context of infinitesimal elasticity, we will employ the notation $\boldsymbol{E}_e$ in this section to represent the internal elastic strains in both cases. Models that make use of the linearized formulation are discussed in, for example, Refs. [31] and [32] for viscoelasticity based on strain-like internal variables and Refs. [16] and [27] for viscoelasticity based on stress-like internal variables.

Introducing Eq. (116) in the viscous flow rule of Eq. (80) we obtain

$$-\left. \frac{d\boldsymbol{E}_e}{dt} \right|_{\dot{\boldsymbol{E}}=\boldsymbol{0}} = \mathbb{P}^S : \underbrace{\left(\sum_i^3 \sum_j^3 \frac{1}{\tau_{ij}} \boldsymbol{L}_{ij}^S \otimes \boldsymbol{L}_{ij}^S \right)}_{\mathbb{T}^{-1}} : \mathbb{P}^S : \boldsymbol{E}_e$$

$$\tag{118}$$

where the relaxation times τ_{ij} are defined in Eq. (88). Even though $\mathbb{V}^{-1}$ has been assumed isotropic, note that an orthotropic viscoelastic behavior (linear in logarithmic, or infinitesimal, strains) is obtained in terms of a fourth-order deviatoric orthotropic *relaxation* tensor $\mathbb{T}_d^{-1} := \mathbb{P}^S : \mathbb{T}^{-1} : \mathbb{P}^S$, where $\mathbb{T}^{-1}$ is "diagonal" (in its matrix representation in preferred axes) and includes the six different, but not independent, relaxation times τ_{ij}. Equation (118) is to be directly compared to its one-dimensional, infinitesimal version given in Eq. (13). Furthermore, even though Eqs. (86) and (118) seem identical, the difference in nature between them must be emphasized: Eq. (86) is only a particularization of the general non-linear constitutive Equation (80) used to determine the viscosity constant η^d from experimental data, whereas Eq. (118) represents the constitutive equation itself for the non-equilibrated part of the Finite Linear Viscoelasticity models. The former is only employed to arrive at Eq. (89), whereas the latter is the equation employed to integrate the strains in the particular linear case of this Section.

The integration of Eq. (118) gives an explicit update for ${}^{t+\Delta t}_0 \boldsymbol{E}_e$ in terms of ${}^{tr}\boldsymbol{E}_e$, i.e. —compare to Eq. (81) for the non-linear case

$$\left(\mathbb{I}^S + \Delta t \mathbb{T}_d^{-1} \right) : {}^{t+\Delta t}_0 \boldsymbol{E}_e = {}^{tr}\boldsymbol{E}_e \tag{119}$$

or

$${}^{t+\Delta t}_0 \boldsymbol{E}_e = \left(\mathbb{I}^S + \Delta t \mathbb{T}_d^{-1} \right)^{-1} : {}^{tr}\boldsymbol{E}_e \tag{120}$$

so the local Newton iterations at the quadrature points of the finite-element discretization, see Section 5.3, are not needed. We observe again that ${}^{t+\Delta t}_0 \boldsymbol{E}_e$ and ${}^{tr}\boldsymbol{E}_e$ are traceless and that they do not have the same principal basis due to the orthotropic nature of the fourth-order deviatoric relaxation tensor $\mathbb{T}_d^{-1}$.

Finally, for pure isotropic behavior $\mu_{ij}^{neq} = \mu^{neq}$, so only one relaxation time $\tau = \eta^d/\mu^{neq}$ is obtained, as one would expect. Then

$$\mathbb{T}_d^{-1} = \mathbb{P}^S : \mathbb{T}^{-1} : \mathbb{P}^S = \mathbb{P}^S : \frac{1}{\tau}\mathbb{I}^S : \mathbb{P}^S = \frac{1}{\tau}\mathbb{P}^S \tag{121}$$

and the "return mapping" for the elastic deviatoric logarithmic strains becomes linear isotropic:

$$^{t+\Delta t}_{0}\boldsymbol{E}_e = \frac{1}{1 + \dfrac{\Delta t}{\tau}} \, ^{tr}\boldsymbol{E}_e \qquad (122)$$

with $^{t+\Delta t}_{0}\boldsymbol{E}_e$ and $^{tr}\boldsymbol{E}_e$ being coaxial in this particular case. This last equation clearly represents the extension of Eq. (20) to the context of isotropic incompressible finite linear viscoelasticity based either on linear logarithmic stress-strain relations or on infinitesimal elasticity for the non-equilibrated response.

6 Equilibrated contribution

If the total gradient $^{t+\Delta t}_{0}\boldsymbol{X}$ is known at the time step $t+\Delta t$, then the equilibrated contributions $^{t+\Delta t}\boldsymbol{S}_{eq}$ and $^{t+\Delta t}\mathbb{C}_{eq}$ are just obtained from $\Psi_{eq}(\boldsymbol{E})$ as hyperelastic calculations, i.e.

$$\boldsymbol{S}_{eq} = \frac{d\Psi_{eq}}{d\boldsymbol{A}} = \frac{d\Psi_{eq}}{d\boldsymbol{E}} : \frac{d\boldsymbol{E}}{d\boldsymbol{A}} = \boldsymbol{T}_{eq} : \frac{d\boldsymbol{E}}{d\boldsymbol{A}} \qquad (123)$$

$$\mathbb{C}_{eq} = \frac{d\boldsymbol{S}_{eq}}{d\boldsymbol{A}} = \frac{d\boldsymbol{E}}{d\boldsymbol{A}} : \frac{d\boldsymbol{T}_{eq}}{d\boldsymbol{E}} : \frac{d\boldsymbol{E}}{d\boldsymbol{A}} + \boldsymbol{T}_{eq} : \frac{d^2\boldsymbol{E}}{d\boldsymbol{A}d\boldsymbol{A}} \quad (124)$$

Furthermore, since $\Psi_{eq}(\boldsymbol{E}) = \mathcal{W}_{eq}(\boldsymbol{E}^d) + \mathcal{U}_{eq}(J)$, the computation of $\boldsymbol{S}_{eq}$ and $\mathbb{C}_{eq}$ can also be conveniently separated into their respective deviatoric and volumetric parts. These computations do not bring about further difficulties, so we omit further details in this work. The interested reader can see the detailed formulae needed to compute these (hyperelastic) contributions for nearly-incompressible orthotropic materials in Ref. [59], Section 2.5.

7 Determination of the relaxation time(s) of the orthotropic model

Consider a small strains uniaxial relaxation test performed about the preferred material direction $\boldsymbol{a}_1$ of an incompressible material. Equation (86) represented in preferred material axes and specialized at $t = 0^+$ (just after the total deformation in direction $\boldsymbol{a}_1$ is applied and retained) reads —note that shear terms are not needed and that $\boldsymbol{\varepsilon}_e^0 = \boldsymbol{\varepsilon}_e(t=0^+) = \boldsymbol{\varepsilon}(t=0^+) = \boldsymbol{\varepsilon}^0$ are isochoric (traceless)

$$-\begin{bmatrix} \dot{\varepsilon}_{e11}^0 \\ \dot{\varepsilon}_{e22}^0 \\ \dot{\varepsilon}_{e33}^0 \end{bmatrix}_{\dot{\varepsilon}=0} = \frac{1}{3} \begin{bmatrix} 2 & -1 & -1 \\ -1 & 2 & -1 \\ -1 & -1 & 2 \end{bmatrix} \begin{bmatrix} \varepsilon_{11}^0/\tau_{11} \\ \varepsilon_{22}^0/\tau_{22} \\ \varepsilon_{33}^0/\tau_{33} \end{bmatrix}$$
$$= \frac{\varepsilon_{11}^0}{3\eta^d} \begin{bmatrix} 2\mu_{11}^{neq} + \mu_{22}^{neq}\nu_{12}^0 + \mu_{33}^{neq}\nu_{13}^0 \\ -\mu_{11}^{neq} - 2\mu_{22}^{neq}\nu_{12}^0 + \mu_{33}^{neq}\nu_{13}^0 \\ -\mu_{11}^{neq} + \mu_{22}^{neq}\nu_{12}^0 - 2\mu_{33}^{neq}\nu_{13}^0 \end{bmatrix} \quad (125)$$

where the relations of Eq. (88) have been used and the initial Poisson ratios $\nu_{12}^0 = -\varepsilon_{22}^0/\varepsilon_{11}^0$ and $\nu_{13}^0 = -\varepsilon_{33}^0/\varepsilon_{11}^0$ are expressed below in terms of the equilibrated and non-equilibrated reference shear moduli.

Stresses at $t = 0^+$ are obtained through —note that in infinitesimal kinematics there is no distinction among stress tensors

$$\boldsymbol{\sigma}^0 = \boldsymbol{\sigma}_{eq}^0 + \boldsymbol{\sigma}_{neq}^0 = \left.\frac{d\mathcal{W}_{eq}}{d\boldsymbol{\varepsilon}}\right|_{\boldsymbol{\varepsilon}^0} + \left.\frac{d\mathcal{W}_{neq}}{d\boldsymbol{\varepsilon}_e}\right|_{\boldsymbol{\varepsilon}^0} + p^0\,\boldsymbol{I} \quad (126)$$

where p^0 is the (initial) hydrostatic pressure needed to fulfill the boundary conditions. In matrix notation we can write

$$\begin{bmatrix} \sigma_{11}^0 \\ 0 \\ 0 \end{bmatrix} = \varepsilon_{11}^0 \begin{bmatrix} 2\mu_{11}^0 + \hat{p}^0 \\ -2\mu_{22}^0\nu_{12}^0 + \hat{p}^0 \\ -2\mu_{33}^0\nu_{13}^0 + \hat{p}^0 \end{bmatrix} \quad (127)$$

where

$$\mu_{ii}^0 = \mu_{ii}^{eq} + \mu_{ii}^{neq} \quad \text{(no sum on } i) \qquad (128)$$

and we have defined $\hat{p}^0 := p^0/\varepsilon_{11}^0$. The boundary conditions $\sigma_{22}^0 = \sigma_{33}^0 = 0$, together with the incompressibility constraint $1 - \nu_{12}^0 - \nu_{13}^0 = 0$, let us obtain the expression of the modified pressure $\hat{p}^0$ and also the Poisson ratios

$$\nu_{12}^0 = \frac{\mu_{33}^0}{\mu_{22}^0 + \mu_{33}^0} = \frac{\mu_{33}^{eq} + \mu_{33}^{neq}}{\mu_{22}^{eq} + \mu_{22}^{neq} + \mu_{33}^{eq} + \mu_{33}^{neq}} \quad (129)$$

$$\nu_{13}^0 = \frac{\mu_{22}^0}{\mu_{22}^0 + \mu_{33}^0} = \frac{\mu_{22}^{eq} + \mu_{22}^{neq}}{\mu_{22}^{eq} + \mu_{22}^{neq} + \mu_{33}^{eq} + \mu_{33}^{neq}} \quad (130)$$

The stress component σ_{11}^0 is then

$$\sigma_{11}^0 = \left(2\mu_{11}^0 + \mu_{22}^0\nu_{12}^0 + \mu_{33}^0\nu_{13}^0\right)\varepsilon_{11}^0 =: E_{11}^0\varepsilon_{11}^0 \quad (131)$$

where we identify E_{11}^0 as the instantaneous Young's modulus in direction $\boldsymbol{a}_1$.

In order to determine the relaxation time τ_{11} we need previously to obtain the expression of the time derivative of the relaxation curve $\sigma_{11}(t)$ at $t = 0^+$. To this end, it is convenient to rewrite Eq. (131) as —note that the same initial Poisson's ratios $\nu_{12}^0 = -\varepsilon_{22}^0/\varepsilon_{11}^0 = -\varepsilon_{e22}^0/\varepsilon_{e11}^0$ and $\nu_{13}^0 = -\varepsilon_{33}^0/\varepsilon_{11}^0 = -\varepsilon_{e33}^0/\varepsilon_{e11}^0$ are to be used in order to define the equilibrated and non-equilibrated instantaneous Young's moduli E_{11}^{eq} and E_{11}^{neq}

$$\sigma_{11}^0 = \underbrace{\left(2\mu_{11}^{eq} + \mu_{22}^{eq}\nu_{12}^0 + \mu_{33}^{eq}\nu_{13}^0\right)}_{E_{11}^{eq}} \varepsilon_{11}^0$$
$$+ \underbrace{\left(2\mu_{11}^{neq} + \mu_{22}^{neq}\nu_{12}^0 + \mu_{33}^{neq}\nu_{13}^0\right)}_{E_{11}^{neq}} \varepsilon_{e11}^0 \quad (132)$$

whereupon

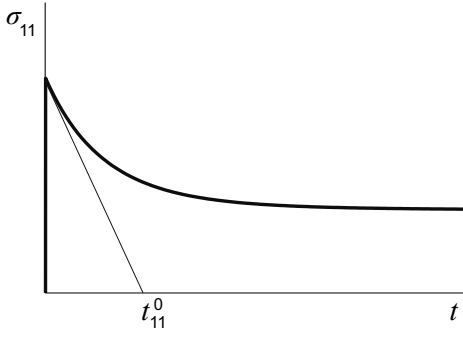$$\dot{\sigma}_{11}^0 = E_{11}^{neq}\dot{\varepsilon}_{e11}^0 \qquad (133)$$

Fig. 4 Determination of the experimental factor $t_{11} = -\sigma_{11}^0/\dot\sigma_{11}^0$ from the curve $\sigma_{11}(t)$ obtained from a uniaxial relaxation test performed about the preferred material direction a_1.
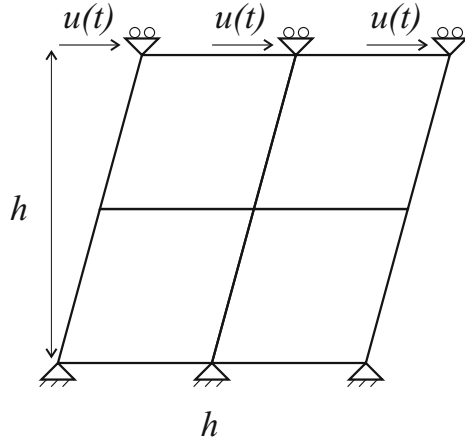

Fig. 5 Cyclic shear of a square $(h \times h)$ specimen under plane strain. Mesh discretization, boundary conditions and applied displacements $u(t) = u_0 \sin(\omega t)$ [31].

because of $\varepsilon_{11}(t) = \varepsilon_{11}^0$ is retained for $t > 0$. Inserting the first component of Eq. (125), with $\eta^d = \tau_{11}\mu_{11}^{neq}$, into Eq. (133) gives

$$\dot\sigma_{11}^0 = -\frac{1}{\tau_{11}}\frac{E_{11}^{neq}}{3\mu_{11}^{neq}}E_{11}^{neq}\varepsilon_{11}^0 \qquad (134)$$

Therefore, by direct comparison of Eqs. (131) and (134), with $E_{11}^0 = E_{11}^{eq} + E_{11}^{neq}$ and $t_{11}^0 := -\sigma_{11}^0/\dot\sigma_{11}^0$, we arrive to

$$\tau_{11} = t_{11}^0 \frac{E_{11}^{neq}/(3\mu_{11}^{neq})}{1 + E_{11}^{eq}/E_{11}^{neq}} \qquad (135)$$

where the numerical value t_{11}^0 may be measured tracing the tangent to the experimental relaxation curve $\sigma_{11}(t)$ at $t = 0^+$, see Figure 4. For further use, we can generalize Eq. (135) to give the expression of the relaxation time τ_{ii} (no sum on i) associated to the preferred direction a_i, i.e. for $i \neq j \neq k \neq i = \{1,2,3\}$ and not applying the summation convention

$$\tau_{ii} = t_{ii}^0 \frac{E_{ii}^{neq}/(3\mu_{ii}^{neq})}{1 + E_{ii}^{eq}/E_{ii}^{neq}} \qquad (136)$$

with

$$t_{ii}^0 = -\sigma_{ii}^0/\dot\sigma_{ii}^0 \qquad (137)$$

$$E_{ii}^{neq} = 2\mu_{ii}^{neq} + \mu_{jj}^{neq}\nu_{ij}^0 + \mu_{kk}^{neq}\nu_{ik}^0 \qquad (138)$$

$$E_{ii}^{eq} = 2\mu_{ii}^{eq} + \mu_{jj}^{eq}\nu_{ij}^0 + \mu_{kk}^{eq}\nu_{ik}^0 \qquad (139)$$

and

$$\nu_{ij}^0 = \frac{\mu_{kk}^0}{\mu_{jj}^0 + \mu_{kk}^0} = \frac{\mu_{kk}^{eq} + \mu_{kk}^{neq}}{\mu_{jj}^{eq} + \mu_{jj}^{neq} + \mu_{kk}^{eq} + \mu_{kk}^{neq}} \qquad (140)$$

Recall that we can only characterize one relaxation time τ_{ii} (i.e. only one isotropic viscosity $\eta^d = \tau_{ii}\mu_{ii}^{neq}$) from experimental data. Subsequently, the remaining relaxation times predicted by the model for axial and shear behaviors are given by Eqs. (88) or (90). Finally,

for the case of incompressible isotropic viscoelasticity we get the single value $\nu^0 = 1/2$, hence $E^{eq} = 3\mu^{eq}$ and $E^{neq} = 3\mu^{neq}$, and we recover the usual value in all directions—compare to the compressible model of Ref. [15]

$$\tau = \frac{t^0}{1 + E^{eq}/E^{neq}} = \frac{t^0}{1 + \mu^{eq}/\mu^{neq}} \qquad (141)$$

with the special case $\tau \approx t^0$ for $\mu^{neq} \gg \mu^{eq}$.

8 Examples

In the following examples we make use of the spline-based strain energy functions described in Refs. [70] and [59] for isotropic and orthotropic incompressible hyperelasticity, respectively. We see below that with this hyperelastic models we are able to capture the equilibrated and non-equilibrated behaviors in an exact way. As an additional material parameter, a relaxation time obtained from a relaxation test about a specific preferred material direction will also be needed in order to complete the definition of the model.

8.1 Isotropic material

In the first example of Ref. [31] a square specimen under a plane strain state is subjected to cyclic shear loading, see Figure 5, where $u(t) = u_0 \sin(\omega t)$. In the present example we reproduce the results of the simulations of that paper using the general formulation for nearly incompressible materials presented in the preceding Sections in order to show that it gives the same results that the isotropic formulation in principal strain directions derived in [31].

First, we use the spline-based hyperelastic formulation for incompressible isotropic materials (see Ref. [70]) to obtain two strain energy functions $\mathcal{W}_{eq}$ and $\mathcal{W}_{neq}$ expressed in terms of principal deviatoric logarithmic strains, i.e.

$$\mathcal{W}_{eq}(\boldsymbol{E}^d) = \omega_{eq}(E_1^d) + \omega_{eq}(E_2^d) + \omega_{eq}(E_3^d) \qquad (142)$$

$$\mathcal{W}_{neq}(\boldsymbol{E}_e^d) = \omega_{neq}(E_{e1}^d) + \omega_{neq}(E_{e2}^d) + \omega_{neq}(E_{e3}^d) \quad (143)$$

that exactly replicate the respective stresses associated to the two Ogden-type energy functions used in the first example of Ref. [31]. Note that, actually, we would determine these functions from experimental data from, first, an instantaneous test (from which we would determine $\mathcal{W} = \mathcal{W}_{eq} + \mathcal{W}_{neq}$) and, second, a sufficiently slow test (from which we would determine $\mathcal{W}_{eq}$). However, we want to predict the results of Ref. [31] using our model. In Figure 6 the (analytical) stresses from the respective uniaxial tests obtained using the Ogden strain energy functions are shown. Subsequently, from discrete representations of those curves, two respective spline-based strain energy functions $\mathcal{W}_{eq}$ and $\mathcal{W}_{neq}$ are obtained separately (not shown). Finally, in Figure 6 the stresses predicted by each spline-based strain energy function are shown. The fact that both stress distributions are exactly replicated indicates that the spline-based functions $\mathcal{W}_{eq}$ and $\mathcal{W}_{neq}$ that we use in the finite-element calculations are equivalent to those used by the authors in Ref. [31]. Note that all of these functions, spline type and Ogden type, are based on the same additive decomposition, i.e. the Valanis-Landel hypothesis. Of course we could have equally used the Ogden model, but an additional purpose of this example is to show the capabilities of the spline-based energy functions, where no material parameter is employed and the behavior is exactly captured. On the other hand, we prescribe the same relaxation time provided in that Reference, i.e. $\tau = 17.5\,\mathrm{s}$, so almost identical final results are expected to be obtained if the same finite element formulation is employed.

The only difference between our strain energy proposal (see Eqs. (60)–(61)) and the one of Ref. [31] is that Reese and Govindjee initially assume volumetric functions for both the equilibrated and the non-equilibrated stored energy contributions (see Eq. (56) of that Reference). However, Reese and Govindjee neglect the non-equilibrated volumetric part of the evolution equation in all the numerical calculations that they perform in order to gain computational efficiency. Hence, the strain energy proposals used in their calculations and our calculations become the same. We have seen above that if a non-equilibrated volumetric part is not initially considered, then the viscous flow is deviatoric, as it should

be for a totally incompressible material. Thus, we note that we neglect that contribution from purely physical grounds. Since only one volumetrical contribution is considered, the same mixed formulation [71] used to avoid mesh locking in nearly-incompressible hyperelastic numerical calculations (cf. [59]) may be used herein. That is, all the variables needed to interpolate the pressure at each finite-element are obtainable from Section 6; further modifications due to the non-equilibrated deviatoric contribution to stress and tangent are not required.

In this bi-dimensional example we employ the 4/1 quad element (or $Q1/P0$ element) for u/p mixed formulation [64] in order to perform proper comparisons to the results of Ref. [31] (because in the first example of Ref. [31] the authors have used four elements with four displacement nodes each). We also assume that the volumetric penalty function of the equilibrated part $\mathcal{U}_{eq}(J)$ used in Ref. [31] is the same that the authors indicate for the non-equilibrated part, i.e.

$$\mathcal{U}_{eq}(J) = \frac{\kappa_{eq}}{4}\left(J^2 - 2\ln J - 1\right) \qquad (144)$$

where κ_{eq} is the bulk modulus. The exact numerical value assigned to the penalty parameter κ_{eq} is not provided in the example under study of that reference, so high enough ratios κ_{eq}/μ_{eq} are chosen so that (nearly-) incompressibility is attained at each case. The reference shear modulus μ_{eq} is readily obtained from the spline-based strain energy function $\mathcal{W}_{eq}$ through

$$\mu_{eq} = \frac{1}{2}\left.\frac{\partial^2 \mathcal{W}_{eq}}{(\partial E^d)^2}\right|_{lin} = \frac{1}{2}\left.\frac{\partial^2 \mathcal{W}_{eq}}{(\partial E^d)^2}\right|_{E^d=0} = \frac{1}{2}\omega_{eq}''(0) \qquad (145)$$

In Figure 7, the Cauchy shear stresses $\sigma_{12}(t)$ are plotted against the engineering shear strains $\gamma_{12}(t) = u(t)/h = u_0/h \times \sin(0.3t)$ for four amplitudes $u_0/h = \{0.01, 1, 2, 5\}$. For these simulations, 50 time steps per cycle have been chosen.

No difference can be appreciated between these results and those presented in Figure 3$(a-d)$ of Ref. [31], even though both the formulation and the strain energy functions are "different". Obviously, all the conclusions reached in that paper regarding the non-linear and linearized formulations are also applicable to our model, which is essentially the same model of Reese and Govindjee but formulated using a more general approach that makes possible its extension to anisotropic materials, as we show in the next examples.
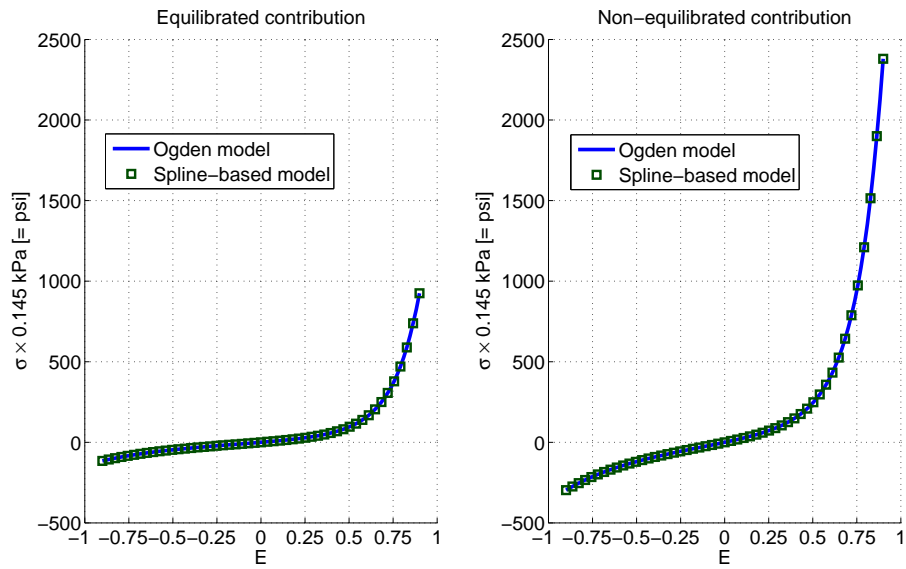
Fig. 6 Uniaxial stresses from the equilibrated and non-equilibrated Ogden-type strain energy functions given in the first example of Ref. [31] and exact fitting of that data using the respective spline-based strain energy functions.
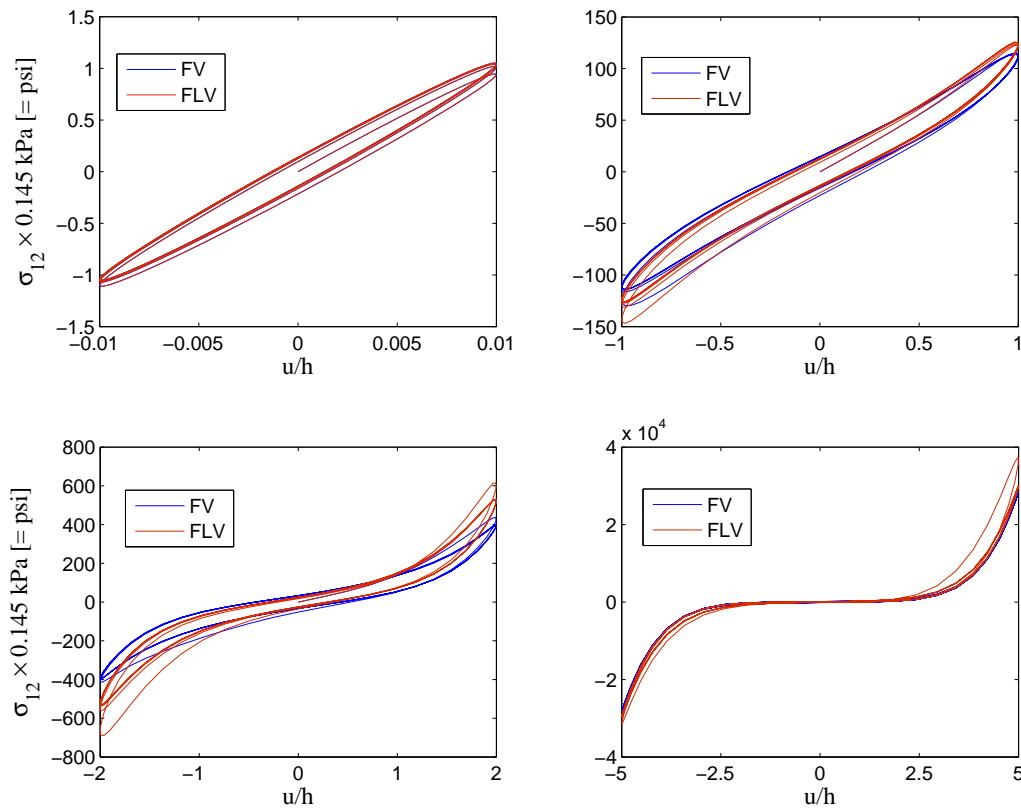

Fig. 7 Cauchy shear stresses $\sigma_{12}(t)$ versus engineering shear strains $\gamma_{12}(t) = u(t)/h = u_0/h \times \sin(0.3t)$ for the amplitudes: a) $u_0/h = 0.01$, b) $u_0/h = 1$, c) $u_0/h = 2$, d) $u_0/h = 5$. No differences are observable with respect to the results of the first example of Ref. [31]. $FV \equiv$ finite (non-linear) viscoelasticity case; $FLV \equiv$ finite linear viscoelasticity case.

8.2 Orthotropic material with linear logarithmic stress-strain relations

In this example we perform three relaxation tests using the finite linear viscoelasticity model explained in Section 5.5 in order to show that the computational results predict the relaxation times given by Eq. (136), together with the Poisson's ratios of Eq. (140), and also agree with the existing relations between the relaxation times given by Eq. (90).

Consider the following strain energy functions

$$\mathcal{W}_{eq}(\boldsymbol{E}^d) = \mu_{11}^{eq}(E_{11}^d)^2 + \mu_{22}^{eq}(E_{22}^d)^2 + \mu_{33}^{eq}(E_{33}^d)^2 \quad (146)$$

$$\mathcal{W}_{neq}(\boldsymbol{E}_e^d) = \mu_{11}^{neq}(E_{e11}^d)^2 + \mu_{22}^{neq}(E_{e22}^d)^2 + \mu_{33}^{neq}(E_{e33}^d)^2 \tag{147}$$

where only their axial components in principal material directions are needed in order to simulate the different uniaxial relaxation tests about the preferred material axes. We take, for example, the following values for the shear moduli in Eqs. (146) and (147)

$$\mu_{11}^{eq} = 4\,\text{MPa}\,,\ \mu_{22}^{eq} = 2\,\text{MPa}\,,\ \mu_{33}^{eq} = 1\,\text{MPa} \tag{148}$$

$$\mu_{11}^{neq} = 5\,\text{MPa}\,,\ \mu_{22}^{neq} = 3\,\text{MPa}\,,\ \mu_{33}^{neq} = 2\,\text{MPa} \tag{149}$$

Finally, the value of the relaxation time $\tau_{11} = 20\,\text{s}$ completes the definition of the model.

In Figure 8 the undeformed (at $t = 0$) and deformed (at $t = 0^+$) configurations of the specimen being tested are shown. In this first computational calculation, the specimen has been stretched in the material direction 1 up to $\lambda_1 = 3$ with the lateral faces being stress-free. Subsequently, the stretch $\lambda_1 = 3$ is maintained 250 s, so the normal stresses in direction $\boldsymbol{a}_1$ and the transverse strains in directions $\boldsymbol{a}_2$ and $\boldsymbol{a}_3$ relax up to the statically equilibrated configuration ($t \to \infty$). The time steps have been chosen as follows: $\Delta t = 0.1\,\text{s}$ for $0^+ \le t \le 5\,\text{s}$, $\Delta t = 0.5\,\text{s}$ for $5\,\text{s} < t \le 20\,\text{s}$ and $\Delta t = 2\,\text{s}$ for $20\,\text{s} < t \le 250\,\text{s}$. The volumetric penalty function of the equilibrated part $\mathcal{U}_{eq}(J)$ employed in this case is

$$\mathcal{U}_{eq}(J) = \frac{\kappa_{eq}}{2}(J-1)^2 \tag{150}$$

with $\kappa = 10^4\,\text{MPa}$. The deformation is uniform, so only one u/p mixed finite element (8/1 or $Q1/P0$ brick) has been used in the simulations.

The relaxation curve $\sigma_{11}(t)$ that has been obtained is shown in Figure 9 (in red). The value t_{11}^0 used in Eq. (135) is easily measured from that graph, see Figure 4.
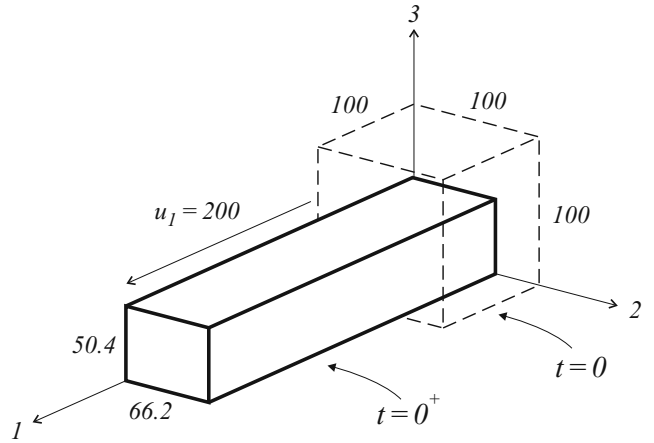

Fig. 8 Uniaxial relaxation test in material direction $\boldsymbol{a}_1$. Configurations at $t = 0$ and $t = 0^+$. Only the displacement $u_1 = 200\,\text{mm}$ ($\lambda_1 = 3$) is prescribed for $t > 0$. Different transverse deformations in directions $\boldsymbol{a}_2$ and $\boldsymbol{a}_3$ are obtained at $t = 0^+$ (indicated in the figure) as a consequence of the single imposed elongation in direction $\boldsymbol{a}_1$ and the material orthotropy. The transverse deformations relax for $t > 0^+$ up to reach the equilibrated state at $t \to \infty$.

Equation (135), with the initial Poisson's ratios given in Eqs. (129) and (130), gives as result

$$\tau_{11}^{test} = 20.1\,\text{s} \tag{151}$$

The fact that the *experimental* ("numerical") relaxation time τ_{11}^{test} obtained from the computed relaxation curve $\sigma_{11}(t)$ at $t = 0^+$ is in very good agreement with the *prescribed* ("theoretical") relaxation time τ_{11} (with a difference of 0.5%) shows that Eq. (135) is consistent with the present finite linear formulation. Thus, inversely, Eq. (135) can be used in an actual situation in which τ_{11} is initially unknown in order to properly characterize the model by means of an experimental relaxation curve $\sigma_{11}(t)$ (usually obtained at small strains). Then, we can take $\tau_{11} = \tau_{11}^{test}$ and the viscosity parameter η^d, needed to perform further finite non-linear viscoelasticity simulations, is just taken as $\eta^d = \tau_{11}^{test}\mu_{11}^{neq}$.

The curves $\sigma_{22}(t)$ and $\sigma_{33}(t)$ corresponding to uniaxial relaxation tests in the other preferred directions are also shown in Figure 9. Equations (136)–(140) give the results

$$\tau_{22}^{test} = 33.4\,\text{s}\,,\quad \tau_{33}^{test} = 50.1\,\text{s} \tag{152}$$

On the other hand, we can verify that the reciprocal relations of Eq. (90) are also satisfied

$$\frac{\tau_{22}^{test}}{\tau_{11}^{test}} = 1.66 \approx \frac{\mu_{11}^{neq}}{\mu_{22}^{neq}}\,,\quad \frac{\tau_{33}^{test}}{\tau_{11}^{test}} = 2.49 \approx \frac{\mu_{11}^{neq}}{\mu_{33}^{neq}} \tag{153}$$

Hence, any of these stress relaxation curves obtained from experimental testing (at small strains in general or at large strains for the very specific case of materials
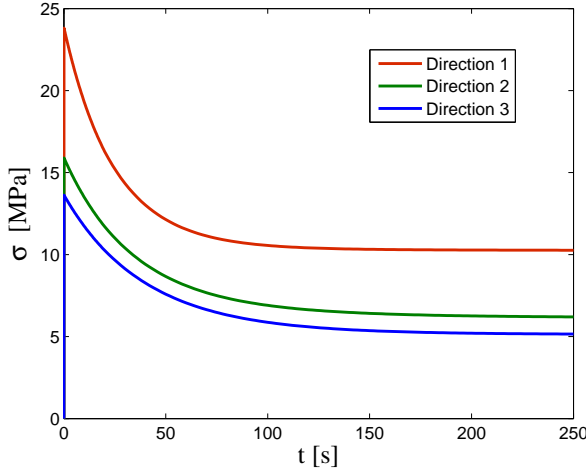
Fig. 9 Stress relaxation curves $\sigma_{11}(t)$, $\sigma_{22}(t)$ and $\sigma_{33}(t)$ obtained from the uniaxial relaxation tests performed about the preferred material directions $\boldsymbol{a}_1$, $\boldsymbol{a}_2$ and $\boldsymbol{a}_3$, respectively.

with linear logarithmic constitutive relations) may be used to characterize the model by means of the viscosity $\eta^d = \tau_{ii}^{test} \mu_{ii}^{neq}$ $(i = 1, 2, 3)$.

Finally, as expected, note that when the corresponding value t/τ_{ii} is large enough, each curve in Figure 9 tends to its respective equilibrated value σ_{ii}^{eq} —just remove the non-equilibrated constants in Eqs. (128)–(131) and substitute ε by $E = \ln \lambda = \ln 3 = 1.099$

$$\sigma_{11}^{eq} = 10.25\,\mathrm{MPa}\ ,\quad \sigma_{22}^{eq} = 6.15\,\mathrm{MPa}\ ,\quad \sigma_{33}^{eq} = 5.13\,\mathrm{MPa} \tag{154}$$

Accordingly to Eqs. (151) and (152), i.e. $\tau_{11}^{test} < \tau_{22}^{test} < \tau_{33}^{test}$, we observe that the uniaxial stress σ_{11} relaxes faster (in relative terms respect to its initial value) than σ_{22} and that σ_{22} relaxes (slightly) faster than σ_{33}.

8.3 Orthotropic material

In this example we study the use of the presented orthotropic visco-hyperelastic model and algorithm based on material logarithmic strains in non-uniform off-axis deformation cases. Two separated relaxation tests are performed over a three-dimensional plate with a concentric circular hole in which the preferred material axes are not aligned with the test axes. The geometry and finite element discretization of the undeformed plate are depicted in Figure 10. The plate is stretched in x-direction by imposing an instantaneous total elongation of $l = 40\,\mathrm{mm}$ at $t = 0^+$, which is then retained for $t > 0$. We assume perfectly lubricated grips at both ends and a plane strain condition throughout the plate.

The deviatoric responses of the equilibrated and non-equilibrated parts of our model are described by orthotropic spline-based strain energy functions of the type —cf. Ref. [59]

$$\mathcal{W}_{eq}(\boldsymbol{E}^d) = \sum_i^3 \sum_j^3 \omega_{ij}^{eq}(E_{ij}^d) \tag{155}$$

$$\mathcal{W}_{neq}(\boldsymbol{E}_e^d) = \sum_i^3 \sum_j^3 \omega_{ij}^{neq}(E_{eij}^d) \tag{156}$$

where six different terms ω_{ij} are needed for each strain energy function. The volumetric function is given in Eq. (150), in this case with $\kappa = 2 \times 10^3\,\mathrm{MPa}$, and the chosen relaxation time is $\tau_{11} = 10\,\mathrm{s}$. In order to prevent mesh-locking, fully integrated $(3 \times 3 \times 3$ Gauss integration) 27/4, u/p mixed finite elements are used in all the simulations. A standard Newton–Raphson scheme, without line searches, is employed for the incremental (global) solution.

The same off-axis uniaxial test, with the same reference configuration of the plate and loading conditions, is simulated for two different materials. The only difference between these materials is the component $\omega_{12}^{neq}(E_{e12}^d)$ included in the non-equilibrated strain energy function $\mathcal{W}_{neq}(\boldsymbol{E}_e^d)$, i.e. eleven functions ω_{ij} over a total of twelve functions needed to define each material are the same for both materials. However, we will see that very different responses are obtained in both cases, which reveals the importance of using a set of, at least, six curves (as for infinitesimal elasticity) to define an orthotropic strain energy function (equilibrated, non-equilibrated or just purely hyperelastic). Obviously, if less than six behavior curves are used to characterize an orthotropic hyperelastic strain energy function, then details as the ones shown in this example are surely lost in generic computational calculations.

For the first case we have chosen equal strain energy functions for the equilibrated and non-equilibrated parts, i.e. $\mathcal{W}_{eq} = \mathcal{W}_{neq} = \mathcal{W}_I$, where the first derivatives of the components ω_{ij}^I used for both stored energy functions are shown in Figures 11.a and 11.b. The values for these components have been taken from the orthotropic hyperelastic function calculated in the first case of Section 4.3 of Ref. [59], i.e. the case for which $\nu_{12} = 0.3$. The component ω_{12}^I has been intentionally made less stiff than in that Reference in order to increase the overall observed angular distortion ($\gamma_{xy} < 0$ or clockwise angular distortion) undergone by the plate, see Appendix C. In Figure 12, the deformed configurations of the plate at several instants are depicted. For $t = 0^+$ the internal elastic strains are coincident to the total strains, i.e. $\boldsymbol{E}_e^0 = \boldsymbol{E}^0$, so the instantaneous response of the plate is given by the initial strain energy
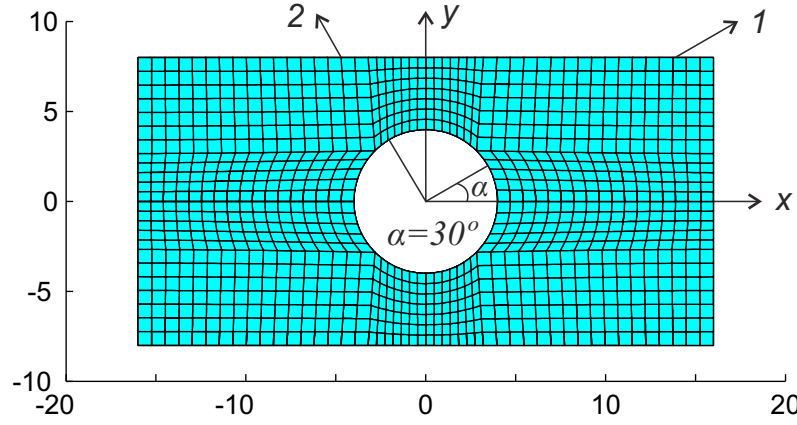
Fig. 10 Rectangular plate with a concentric hole: reference configuration, initial orientation ($\alpha = 30^o$) of the preferred material directions and finite element mesh. Dimensions of the plate: $l_0 \times h_0 \times t_0 = 32 \times 16 \times 0.5 \, \text{mm}^3$. Radius of the hole: $r_0 = 4 \, \text{mm}$.
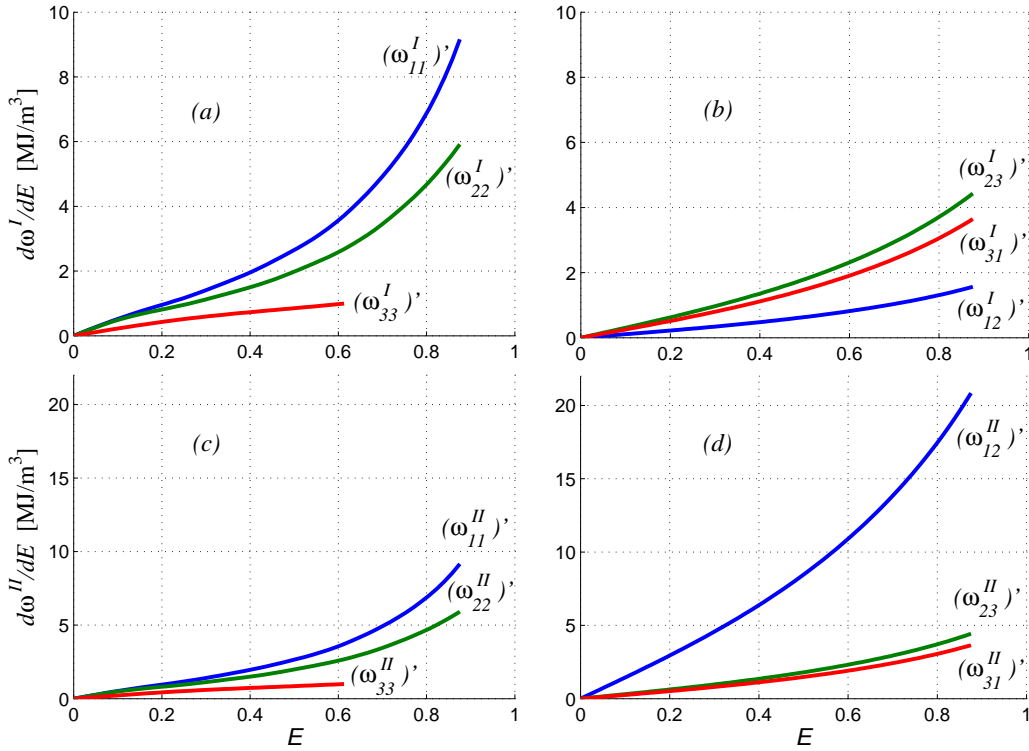

Fig. 11 (a) and (b): First derivatives of the components of the strain energy function $\mathcal{W}_I$. (c) and (d): First derivatives of the components of the strain energy function $\mathcal{W}_{II}$. For the first case addressed in this example (see Figure 12) we use $\mathcal{W}_{eq} = \mathcal{W}_{neq} = \mathcal{W}_I$. For the second case addressed in this example (see Figure 13) we use $\mathcal{W}_{eq} = \mathcal{W}_I$ and $\mathcal{W}_{neq} = \mathcal{W}_{II}$. Note that the only difference between $\mathcal{W}_I$ and $\mathcal{W}_{II}$ is the component ω_{12}. The symmetries $\omega'_{ij}(-E_{ij}) = -\omega'_{ij}(E_{ij})$ are considered for all the functions shown in this figure.

function $\mathcal{W}^0 = \mathcal{W}_{eq} + \mathcal{W}_{neq} = 2\mathcal{W}_I$. On the other hand, for $t \to \infty$ the elastic strains have vanished throughout the plate, so $\mathcal{W}^\infty = \mathcal{W}_{eq} = \mathcal{W}_I = \mathcal{W}^0/2$. Hence, for this case, it is observed that the instantaneous ($t = 0^+$) and relaxed ($t \to \infty$) plate deformations and relative distributions of deviatoric Cauchy stresses are almost identical. The only observed difference between them is that the magnitude of the deviatoric stresses in the initial state is twice the magnitude of the deviatoric stresses in the relaxed state. For $0^+ < t < \infty$, the plate deformation and distribution of stresses over the plate may slightly vary (when compared to the initial and final states) due to the non-uniform evolution of $\boldsymbol{E}_e$ from $t = 0^+$ to $t \to \infty$; see Eq. (80) and notice that the evolution of the elastic strains at a given point depends on the stresses in that point. The time steps have been chosen as follows: $\Delta t = 0.125$ s for $0^+ \le t \le 5$ s and $\Delta t = 1.5$ s for 5 s $< t \le 155$ s.

For the second case being analyzed, the first derivative of the function $\omega_{12}^{neq}(E_{e12}^d)$ of the non-equilibrated contribution is modified as shown in Figure 11.d, i.e. in this case we have $\mathcal{W}_{eq} = \mathcal{W}_I$ (Figures 11.a and 11.b) and $\mathcal{W}_{neq} = \mathcal{W}_{II}$ (Figures 11.c and 11.d). Note that eleven components ω_{ij} (six equilibrated and five non-equilibrated) are exactly the same than in the preceding case. In this case $\mathcal{W}_{eq} \ne \mathcal{W}_{neq}$ and $\mathcal{W}^0 \ne 2\mathcal{W}^\infty$ (even though the initial strains $\boldsymbol{E}_e^0 = \boldsymbol{E}^0$ are again coincident), so the instantaneous and relaxed plate deformations and distributions of stresses are not expected to be equal. In Figure 13, the deformed configuration of the plate and the distribution of deviatoric Cauchy stresses are depicted at several instants. Interestingly, the modification of the single function ω_{12}^{neq} with respect to the previous case makes that the instantaneous overall angular distortion γ_{xy} of the plate at $t = 0^+$ becomes positive. This fact may be easily understood from the small strains theory, see Appendix C. Subsequently, the internal elastic strains and the influence of the modified term ω_{12}^{neq} continuously decrease, so the angular distortion also decreases (relaxes) from the initial (positive) value to the completely relaxed (negative) value. Note that the same equilibrated state is reached in both simulations because both materials have the same equilibrated strain energy function $\mathcal{W}_{eq}(\boldsymbol{E}^d) = \mathcal{W}_I(\boldsymbol{E}^d)$. However, remarkably different instantaneous responses (in terms of plate deformations and magnitude and distribution of stresses) are obtained in both cases. We emphasize that these differences are a consequence of the consideration of just one different curve ω_{12}^{neq} in the strain energy functions of the materials under study.

Tables 1 and 2 show that quadratic force and energy rates of convergence are obtained in typical steps during the computation of the second case addressed in this

Table 1 Asymptotic quadratic convergence: Unbalanced energy and force during a typical computed step of size $\Delta t = 0.125$ s using a Newton–Raphson scheme

Step	Iteration	Force	Energy
20	1/4	1.000E+00	1.000E+00
20	2/4	2.913E−01	8.257E−04
20	3/4	3.401E−03	1.459E−08
20	4/4	2.050E−07	2.267E−16

Table 2 Asymptotic quadratic convergence: Unbalanced energy and force during a typical computed step of size $\Delta t = 1.5$ s using a Newton–Raphson scheme

Step	Iteration	Force	Energy
50	1/4	1.000E+00	1.000E+00
50	2/4	2.669E−01	4.022E−04
50	3/4	3.870E−04	2.634E−09
50	4/4	6.079E−08	4.802E−17

example. In the incremental calculations for the first case, even faster rates of convergence are obtained.

Finally, note that this example has been designed as to let us show the capabilities of the presented orthotropic finite visco-hyperelastic model and at the same time to highlight the importance of considering all twelve experimental curves. In actual situations, the non-equilibrated strain energy function may be completely different to the equilibrated strain energy function and very different instantaneous and final responses may be obtained. In those cases, this model is of course still capable of simulating the relaxation or creep evolutions of those materials.

9 Conclusions

In this paper we have presented a formulation for anisotropic visco-hyperelasticity and a stress-point integration algorithm for finite element analysis. The purely phenomenological formulation is based on the ideas given by Reese and Govindjee for isotropic materials. As proposed by Lubliner, the stored energy is split into an equilibrated part and a nonequilibrated contribution. The only internal variable used by the formulation are the elastic nonequilibrated strains obtained from the nonequilibrated deformation gradient component by the Sidoroff multiplicative decomposition.

The model has been motivated on the small strains formulation for the rheological standard solid. Applications of partial derivatives yielding to elastic-predictor,
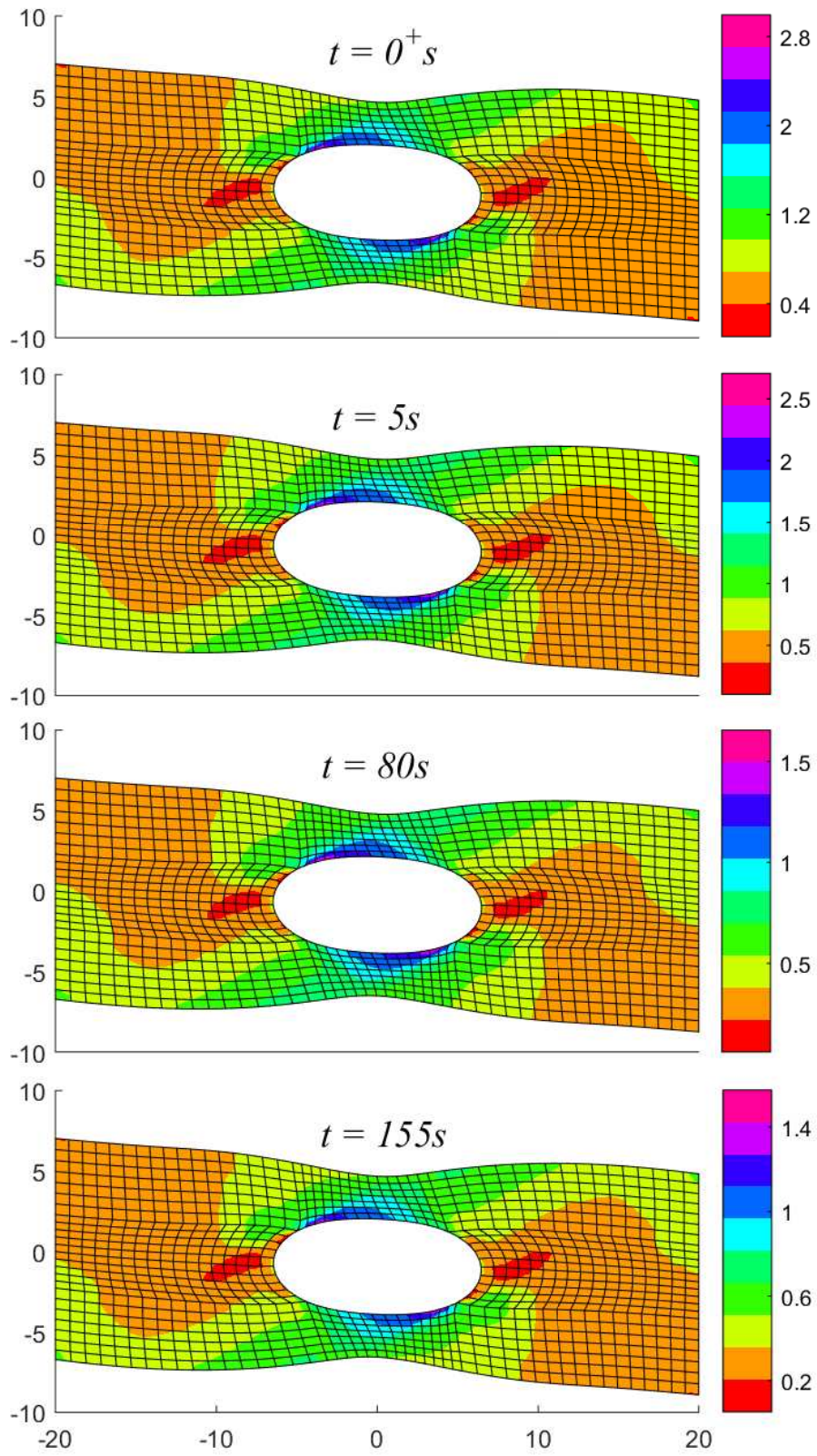
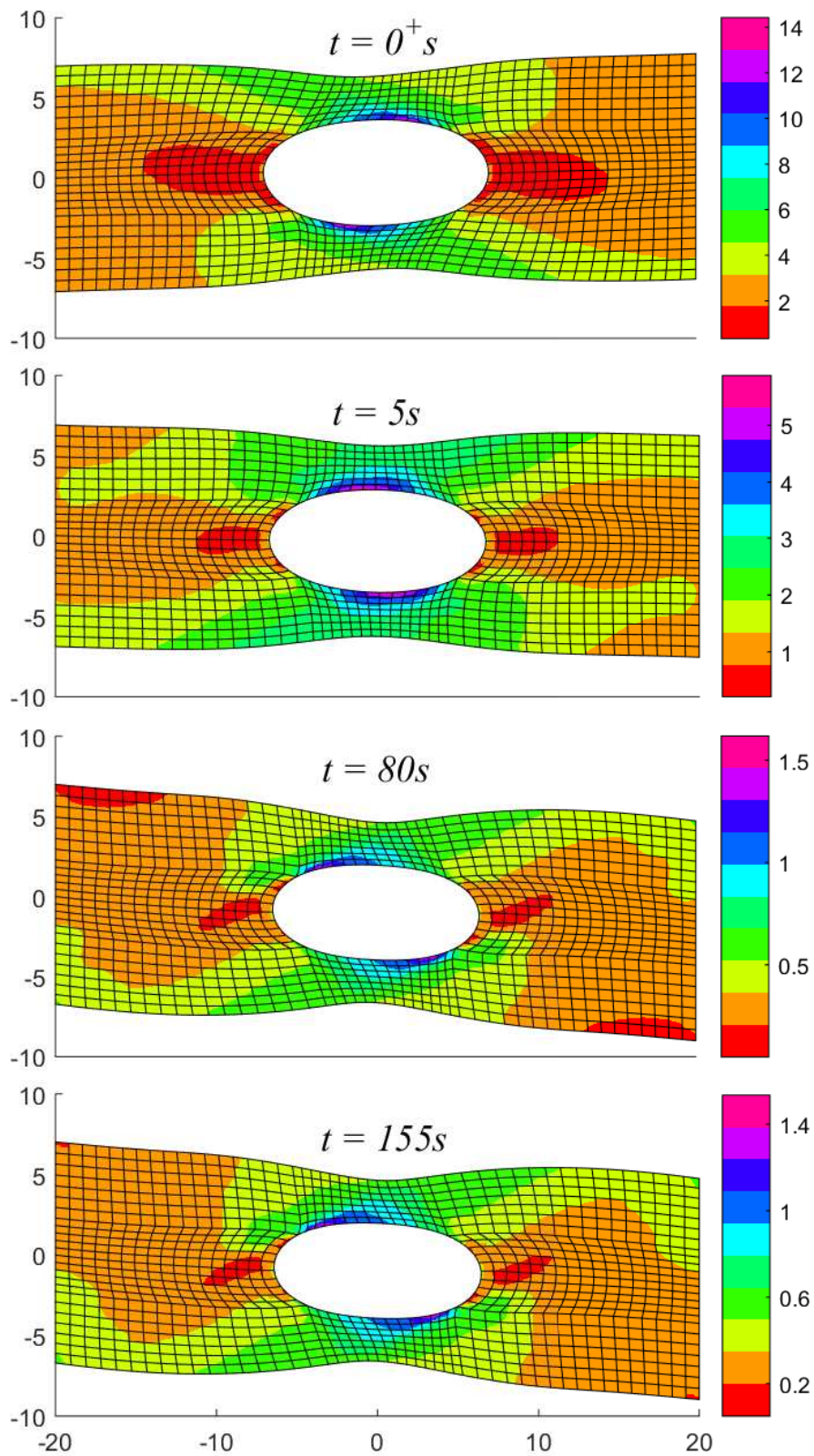**Fig. 12** Relaxation process of the plate with equal equilibrated and non-equilibrated strain energy functions $\mathcal{W}_{eq} = \mathcal{W}_{neq} = \mathcal{W}_I$ (see Figures 11.a and 11.b). Deformed configurations and distributions of $\left\| \boldsymbol{\sigma}^d \right\|$ (MPa) at instants $t = 0^+$ s, $t = 5$ s, $t = 80$ s and $t = 155$ s. Unavereged results at nodes.

Fig. 13 Relaxation process of the plate with equilibrated and non-equilibrated strain energy functions $\mathcal{W}_{eq} = \mathcal{W}_I$ (see Figures 11.a and 11.b) and $\mathcal{W}_{neq} = \mathcal{W}_{II}$ (see Figures 11.c and 11.d), respectively. Deformed configurations and distributions of $\left\|\boldsymbol{\sigma}^d\right\|$ (MPa) at instants $t = 0^+$ s, $t = 5$ s, $t = 80$ s and $t = 155$ s. Unavereged results at nodes.

viscous-corrector algorithms have been carefully introduced in order to extend them to large strain kinematics. Ideas central to the large strains formulation and to the algorithmic development have been given in terms of simpler quadratic stress and strain measures. However, the present formulation has been fully developed in logarithmic strains using mapping tensors in order to directly employ stored energies expressed in such measures. The model is fully nonlinear, i.e. a finite viscoelasticity model and requires local iterations at the integration point level. For the simpler case of finite linear viscoelasticity, no local iterations are needed. The procedure to seamlessly obtain the material parameters has also been explained.

The model may be used with any phenomenological isotropic, transversely isotropic or orthotropic stored energy function. However, greatest advantage may be taken when combined with spline-based stored energies because both the instantaneous and the equilibrium responses may be predicted to a great detail.

The numerical examples show that the computational results are in agreement with the expected ones and that the formulation yields the same response as the Reese and Govindjee formulation for the isotropic case. They also show that the solution may be obtained in few steps achieving second order convergence. A numerical example also emphasizes the importance of all components of the equilibrated and non-equilibrated stored energies in the predictions.

Appendix A: Proof of Eqs. (114) and (115)

The stress tensor $S_{neq}^{|d}$ defined in Eq. (97) is traceless in the sense that

$$S_{neq}^{|d} : C^d = \tau_{neq}^{|d} : I = \tau_{neq}^{|e} : I = T_{neq}^{|e} : I = 0 \quad (157)$$

where the results $\tau_{neq}^{|d} = X^d S_{neq}^{|d} X^{dT} = X^e S_{neq}^{|e} X^{eT} = \tau_{neq}^{|e}$, $tr(\tau_{neq}^{|e}) = tr(T_{neq}^{|e})$ (see Ref. [59]) and Eq. (66) have been used. Therefore, the expression of the second Piola–Kirchhoff stress tensor S_{neq} that derives from the purely deviatoric strain energy function $\mathcal{W}_{neq}$, as given in Eq. (97), reduces to Eq. (114)

$$S_{neq} = S_{neq}^{|d} : J^{-2/3} \left(\mathbb{I} - \frac{1}{3} C^d \otimes C^{d-1} \right)$$
$$= J^{-2/3} S_{neq}^{|d} \quad (158)$$

where $dA^d/dA = dC^d/dC$ has been obtained differentiating the expression $C^d = J^{-2/3}C$, with $J^2 = det(C)$, with respect to C.

Differentiating Eq. (157) with respect to C^d

$$0 = \frac{d(S_{neq}^{|d} : C^d)}{dC^d} = S_{neq}^{|d} : \frac{dC^d}{dC^d} + C^d : \frac{dS_{neq}^{|d}}{dC^d}$$
$$= S_{neq}^{|d} + C^d : \frac{1}{2} \mathbb{C}_{neq}^{|d} \quad (159)$$

Using the major symmetries of $\mathbb{C}_{neq}^{|d}$, cf. Eqs. (102) and (113), we arrive at the following relation

$$S_{neq}^{|d} + \frac{dS_{neq}^{|d}}{dC^d} : C^d = 0 \quad (160)$$

After some algebraic manipulations, we identify this last result in the expression of the deviatoric constitutive tensor that derives from S_{neq}, which finally simplifies to Eq. (115)

$$\mathbb{C}_{neq} = \frac{dS_{neq}}{dA} = 2S_{neq}^{|d} \otimes \frac{dJ^{-2/3}}{dC} + J^{-2/3} \frac{dS_{neq}^{|d}}{dA^d} : \frac{dA^d}{dA}$$
$$= J^{-4/3} \mathbb{C}_{neq}^{|d} \quad (161)$$

Appendix B: General expressions for $T_{neq}^{|tr}$ and $dT_{neq}^{|tr}/d^{tr}E_e$

If the approximation of Eq. (108) is not considered adequate, we can compute the mapping tensor $\partial E_e / \partial^{tr}E_e$ with the viscous flow frozen, needed for the computation of the stresses in Eq. (106), and its gradient with respect to $^{tr}E_e$, needed for the computation of the consistent tangent moduli.

From the relation $^{tr}X_e = X^d \, ^{tr}X_v^{-1}$, with X_v fixed, see Figure 3, we obtain

$$^{tr}d_e = sym(\,^{tr}\dot{X}_e\,^{tr}X_e^{-1}) = sym(\dot{X}^d X^{d-1}) = d^d \quad (162)$$

which represents the spatial counterpart, in rate-form, of the change of variable given in Eq. (99). Accordingly, the independent variables of Eq. (40) may be changed to give

$$d_e\left(\,^{tr}d_e, l_v\right) = \,^{tr}d_e - sym\left(X_e l_v X_e^{-1}\right) \quad (163)$$

or

$$d_e\left(\,^{tr}d_e, l_v\right) = \mathbb{M}_{^{tr}d_e}^{d_e}\Big|_{l_v=0} : \,^{tr}d_e + \mathbb{M}_{l_v}^{d_e}\Big|_{^{tr}d_e=0} : l_v \quad (164)$$

with $\mathbb{M}_{^{tr}d_e}^{d_e}\Big|_{l_v=0} = \mathbb{I}^S$. Hence we obtain —recall Eq. (54)

$$\tau_{neq}^{|e} : d_e\big|_{l_v=0} = \tau_{neq}^{|tr} : \,^{tr}d_e = \tau_{neq}^{|d} : d^d = \dot{\mathcal{W}}_{neq}\Big|_{l_v=0}$$

(165)

with

$$\boldsymbol{\tau}_{neq}^{|tr} = \boldsymbol{\tau}_{neq}^{|e} : \mathbb{M}_{tr\,d_e}^{d_e}\Big|_{\boldsymbol{l}_v=\boldsymbol{0}} = \boldsymbol{\tau}_{neq}^{|e} : \mathbb{I}^S = \boldsymbol{\tau}_{neq}^{|e} \qquad (166)$$

Although $\boldsymbol{\tau}_{neq}^{|e} = \boldsymbol{\tau}_{neq}^{|tr} = \boldsymbol{\tau}_{neq}^{|d}$ represent all them the same Kirchhoff stress tensor operating in the current isochoric configuration, we use different superscripts to emphasize the fact that this stress tensor may be obtained from different Lagrangian stress tensors defined in different configurations. In terms of Generalized Kirchhoff stresses, Eq. (166) reads

$$\boldsymbol{T}_{neq}^{|tr} : \mathbb{M}_{tr\,d_e}^{tr\,\dot{E}_e} = \boldsymbol{T}_{neq}^{|e} : \mathbb{M}_{d_e}^{\dot{E}_e} : \mathbb{M}_{tr\,d_e}^{d_e}\Big|_{\boldsymbol{l}_v=\boldsymbol{0}} \qquad (167)$$

where, for example, $\mathbb{M}_{d_e}^{\dot{E}_e}$ is the fourth-order tensor that maps, on the one hand, the elastic deformation rate tensor $\boldsymbol{d}_e$ to the material rate tensor $\dot{\boldsymbol{E}}_e$ and, on the other hand, the stresses $\boldsymbol{T}_{neq}^{|e}$ to the stresses $\boldsymbol{\tau}_{neq}^{|e}$, compare to Eqs. (45) and (49). Hence

$$\boldsymbol{T}_{neq}^{|tr} = \boldsymbol{T}_{neq}^{|e} : \mathbb{M}_{d_e}^{\dot{E}_e} : \mathbb{M}_{tr\,d_e}^{d_e}\Big|_{\boldsymbol{l}_v=\boldsymbol{0}} : \mathbb{M}_{tr\,\dot{E}_e}^{tr\,d_e} \qquad (168)$$

$$= \boldsymbol{T}_{neq}^{|e} : \mathbb{M}_{tr\,\dot{E}_e}^{\dot{E}_e}\Big|_{\boldsymbol{l}_v=\boldsymbol{0}} = \boldsymbol{T}_{neq}^{|e} : \frac{\partial \boldsymbol{E}_e}{\partial^{\,tr}\boldsymbol{E}_e}\Big|_{\dot{\boldsymbol{X}}_v=\boldsymbol{0}}$$

Taking into consideration that $\mathbb{M}_{tr\,d_e}^{d_e}\Big|_{\boldsymbol{l}_v=\boldsymbol{0}} = \mathbb{I}^S$ we arrive at

$$\frac{\partial \boldsymbol{E}_e}{\partial^{\,tr}\boldsymbol{E}_e}\Big|_{\dot{\boldsymbol{X}}_v=\boldsymbol{0}} = \mathbb{M}_{d_e}^{\dot{E}_e} : \mathbb{M}_{tr\,\dot{E}_e}^{tr\,d_e}$$

$$= \mathbb{M}_{\bar{d}_e}^{\dot{E}_e} : \left(\mathbb{M}_{d_e}^{\bar{d}_e} : \mathbb{M}_{tr\,\bar{d}_e}^{tr\,d_e}\right) : \mathbb{M}_{tr\,\dot{E}_e}^{tr\,\bar{d}_e}$$

$$= \mathbb{M}_{\bar{d}_e}^{\dot{E}_e} : \mathbb{M}_{tr\,\dot{E}_e}^{tr\,\bar{d}_e} \qquad (169)$$

where we have defined the rotated deformation rate tensors

$$\bar{\boldsymbol{d}}_e := \boldsymbol{R}_e^T \odot \boldsymbol{R}_e^T : \boldsymbol{d}_e = \mathbb{M}_{d_e}^{\bar{d}_e} : \boldsymbol{d}_e \qquad (170)$$

$${}^{tr}\bar{\boldsymbol{d}}_e := {}^{tr}\boldsymbol{R}_e^T \odot {}^{tr}\boldsymbol{R}_e^T : {}^{tr}\boldsymbol{d}_e = \mathbb{M}_{tr\,d_e}^{tr\,\bar{d}_e} : {}^{tr}\boldsymbol{d}_e \qquad (171)$$

and we have used the fact that ${}^{tr}\boldsymbol{R}_e = \boldsymbol{R}_e$, so $\mathbb{M}_{d_e}^{\bar{d}_e} : \mathbb{M}_{tr\,\bar{d}_e}^{tr\,d_e} = \mathbb{I}^S$. Thus, the general expression for Eq. (106) reads

$$\boldsymbol{T}_{neq}^{|tr} = \boldsymbol{T}_{neq}^{|e} : \frac{\partial \boldsymbol{E}_e}{\partial^{\,tr}\boldsymbol{E}_e}\Big|_{\dot{\boldsymbol{X}}_v=\boldsymbol{0}} = \boldsymbol{T}_{neq}^{|e} : \mathbb{M}_{\bar{d}_e}^{\dot{E}_e} : \mathbb{M}_{tr\,\dot{E}_e}^{tr\,\bar{d}_e}$$

$$(172)$$

which defines the mapping between the stress tensors $\boldsymbol{T}_{neq}^{|e}$, defined in the updated intermediate configuration, and $\boldsymbol{T}_{neq}^{|tr}$, defined in the trial (fixed) intermediate configuration. The reader is referred to Ref. [59], Eq.

(35), to see the specific spectral form of the mapping tensors present in Eq. (172), where the Lagrangian basis and the stretches are to be adapted to each case. Note that if the deformation occurs about the preferred material directions, then the shear terms of these mapping tensors do not take place in the relation between $\boldsymbol{T}_{neq}^{|tr}$ and $\boldsymbol{T}_{neq}^{|e}$ (because they are coaxial), so from the spectral forms of $\mathbb{M}_{\bar{d}_e}^{\dot{E}_e}$ and $\mathbb{M}_{tr\,\dot{E}_e}^{tr\,\bar{d}_e}$ we obtain $\boldsymbol{T}_{neq}^{|tr} = \boldsymbol{T}_{neq}^{|e}$; recall Eq. $(107)_2$. Furthermore, the approximation of Eq. $(108)_2$ is also based on the specific spectral forms of $\mathbb{M}_{\bar{d}_e}^{\dot{E}_e}$ and $\mathbb{M}_{tr\,\dot{E}_e}^{tr\,\bar{d}_e}$ and on the fact that the eigenvectors of $\boldsymbol{E}_e$ and ${}^{tr}\boldsymbol{E}_e$ are almost coincident for $\Delta t/\tau \ll 1$, as one may deduce from Eq. (81).

For the computation of the consistent tangent moduli $d\boldsymbol{T}_{neq}^{|tr}/d^{\,tr}\boldsymbol{E}_e$, to be used in Eq. (104), we must take into consideration that the trial logarithmic strains ${}^{tr}\boldsymbol{E}_e$ and the updated logarithmic strains ${}^{t+\Delta t}_0\boldsymbol{E}_e$ are related in the algorithm through Eq. (81), so their increments relate through Eq. (111), see also Eq. (112). Then, taking derivatives in Eq. (172) —note that $\mathbb{M}_{\bar{d}_e}^{\dot{E}_e}$ and $\mathbb{M}_{tr\,\dot{E}_e}^{tr\,\bar{d}_e}$ have major and minor symmetries

$$\frac{d\boldsymbol{T}_{neq}^{|tr}}{d^{\,tr}\boldsymbol{E}_e} = \mathbb{M}_{tr\,\dot{E}_e}^{tr\,\bar{d}_e} : \mathbb{M}_{\bar{d}_e}^{\dot{E}_e} : \frac{d\boldsymbol{T}_{neq}^{|e}}{d\boldsymbol{E}_e} : \frac{d^{\,t+\Delta t}_0\boldsymbol{E}_e}{d^{\,tr}\boldsymbol{E}_e}$$

$$+ \mathbb{M}_{tr\,\dot{E}_e}^{tr\,\bar{d}_e} : \left(\boldsymbol{T}_{neq}^{|e} : \frac{d\mathbb{M}_{\bar{d}_e}^{\dot{E}_e}}{d\boldsymbol{E}_e}\right) : \frac{d^{\,t+\Delta t}_0\boldsymbol{E}_e}{d^{\,tr}\boldsymbol{E}_e}$$

$$+ \boldsymbol{T}_{neq}^{|e} : \mathbb{M}_{\bar{d}_e}^{\dot{E}_e} : \frac{d\mathbb{M}_{tr\,\dot{E}_e}^{tr\,\bar{d}_e}}{d^{\,tr}\boldsymbol{E}_e} \qquad (173)$$

or, equivalently

$$\frac{d\boldsymbol{T}_{neq}^{|tr}}{d^{\,tr}\boldsymbol{E}_e} = \frac{\partial \boldsymbol{E}_e}{\partial^{\,tr}\boldsymbol{E}_e}\Big|_{\dot{\boldsymbol{X}}_v=\boldsymbol{0}}^T : \frac{d^2\mathcal{W}_{neq}}{d\boldsymbol{E}_e d\boldsymbol{E}_e} : \frac{d^{\,t+\Delta t}_0\boldsymbol{E}_e}{d^{\,tr}\boldsymbol{E}_e}$$

$$- \frac{\partial \boldsymbol{E}_e}{\partial^{\,tr}\boldsymbol{E}_e}\Big|_{\dot{\boldsymbol{X}}_v=\boldsymbol{0}}^T : \left(\bar{\boldsymbol{\tau}}_{neq}^{|e} : \frac{d\mathbb{M}_{\dot{E}_e}^{\bar{d}_e}}{d\boldsymbol{E}_e}\right) : \frac{d^{\,t+\Delta t}_0\boldsymbol{E}_e}{d^{\,tr}\boldsymbol{E}_e}$$

$$+ \bar{\boldsymbol{\tau}}_{neq}^{|e} : \frac{d\mathbb{M}_{tr\,\dot{E}_e}^{tr\,\bar{d}_e}}{d^{\,tr}\boldsymbol{E}_e} \qquad (174)$$

where the result obtained from taking derivatives with respect to $\boldsymbol{E}_e$ in the identity $\mathbb{M}_{\bar{d}_e}^{\dot{E}_e} : \mathbb{M}_{\dot{E}_e}^{\bar{d}_e} = \mathbb{I}^S$ has been used and $\bar{\boldsymbol{\tau}}_{neq}^{|e}$ stands for the Kirchhoff stress tensor $\boldsymbol{\tau}_{neq}^{|e}$ rotated by $\boldsymbol{R}_e^T$, i.e. $\bar{\boldsymbol{\tau}}_{neq}^{|e} = \boldsymbol{T}_{neq}^{|e} : \mathbb{M}_{\bar{d}_e}^{\dot{E}_e}$. Following customary arguments, the sixth-order tensors of the type $d\mathbb{M}_{\dot{E}}^{\bar{d}}/d\boldsymbol{E}$ present in this last equation may be obtained from the comparison of the spectral decompositions of the material rate of $\mathbb{M}_{\dot{E}}^{\bar{d}}$ and the material rate of $\boldsymbol{E}$, i.e.

$$\dot{\mathbb{M}}_{\dot{E}}^{\bar{d}} = \frac{d\mathbb{M}_{\dot{E}}^{\bar{d}}}{d\boldsymbol{E}} : \dot{\boldsymbol{E}} \qquad (175)$$

see Refs. [49, 59, 72] for similar derivations and further details.

Appendix C: Interpretation of off-axis shearing effects

From the third example above we infer that two different orthotropic materials subjected to the same off-axis finite deformation and with the same orientation of the preferred material axes may undergo angular distortions of opposite sign. Based on the fact that finite logarithmic strains extend the small strains meaning to the large strains setting [46] and on the fact that in that example we are using strain energy functions based on the same invariants used in infinitesimal orthotropic elasticity, we can explain these different mechanical responses from the infinitesimal theory and then extend the results to the case of Example 3.

Consider as an example the uniaxial test of Figure 14 performed over a perfectly incompressible orthotropic material with the preferred material direction 1 oriented at $\alpha = 30^o$ with respect to the test axis x. We consider a plane strain state, so the out-of-plane strains vanish, i.e. $\varepsilon_{31} = \varepsilon_{32} = \varepsilon_{33} = 0$. The in-plane contribution of the (deviatoric) strain energy function is expressed in terms of the components of the infinitesimal strain tensor $\boldsymbol{\varepsilon}$ in the preferred material axes as

$$\mathcal{W}\left(\boldsymbol{\varepsilon}, \boldsymbol{a}_1, \boldsymbol{a}_2\right) = \mu_{11}\varepsilon_{11}^2 + \mu_{22}\varepsilon_{22}^2 + \mu_{12}\left(\varepsilon_{12}^2 + \varepsilon_{21}^2\right) \quad (176)$$

The stresses in principal material directions are

$$\sigma_{11} = 2\mu_{11}\varepsilon_{11} + p \quad (177)$$
$$\sigma_{22} = 2\mu_{22}\varepsilon_{22} + p = -2\mu_{22}\varepsilon_{11} + p \quad (178)$$
$$\sigma_{12} = 2\mu_{12}\varepsilon_{12} = 2\mu_{12}\varepsilon_{21} = \sigma_{21} \quad (179)$$

where the incompressibility constraint $\varepsilon_{22} = -\varepsilon_{11}$ has been used and p is the initially unknown hydrostatic pressure. Since $\sigma_{12} < 0$, Eq. (179) yields $\varepsilon_{12} < 0$. From the Mohr's circle of in-plane stresses shown in Figure 15 we get the relation $\sigma_{11} = 3\sigma_{22}$ (note that the axes $\{x, y\}$ are the principal directions of stresses because $\sigma_{xy} = 0$). Combining Eqs. (177), (178)$_2$ and the relation $\sigma_{11} = 3\sigma_{22}$ we arrive to

$$\sigma_{11} = 3\left(\mu_{11} + \mu_{22}\right)\varepsilon_{11} \quad (180)$$

The sign of the angular distortion $\gamma_{xy} = 2\varepsilon_{xy}$ undergone by the specimen may be obtained by direct comparison of the Mohr's representations of stresses and strains, see Figure 15. On the one hand, in the Mohr's circle of stresses we have $-\sigma_{12}/\left(\sigma_{11}/3\right) = \tan\left(2 \times 30^o\right) = \tan\left(60^o\right)$. On the other hand, from the Mohr's circle in

the strain space we obtain $-\varepsilon_{12}/\varepsilon_{11} = \tan\left(2\theta\right)$. These angles are related by Eqs. (179) and (180), i.e.

$$\frac{-\sigma_{12}}{\sigma_{11}/3} = \frac{2\mu_{12}}{\mu_{11} + \mu_{22}}\frac{-\varepsilon_{12}}{\varepsilon_{11}} \quad (181)$$

Hence we distinguish three different possibilities

$$2\mu_{12} = \mu_{11} + \mu_{22} \;\Rightarrow\; 2\theta = 60^o \;\Rightarrow\; \gamma_{xy} = 0 \quad (182)$$
$$2\mu_{12} > \mu_{11} + \mu_{22} \;\Rightarrow\; 2\theta < 60^o \;\Rightarrow\; \gamma_{xy} > 0 \quad (183)$$
$$2\mu_{12} < \mu_{11} + \mu_{22} \;\Rightarrow\; 2\theta > 60^o \;\Rightarrow\; \gamma_{xy} < 0 \quad (184)$$

which, note, satisfactorily explain the different behaviors obtained for the instantaneous (equilibrated plus non-equilibrated) and equilibrated responses in the Example 3 above. Finally, we remark that the condition $2\mu_{12} = \mu_{11} + \mu_{22}$ does not imply isotropic behavior in the plane 12. Evidently, if the material is isotropic in the plane 12, then $\mu_{11} = \mu_{22} = \mu_{12}$ and the condition $2\mu_{12} = \mu_{11} + \mu_{22}$ is also satisfied, as one would expect.

Interestingly, the strain components ε_{xx} and ε_{xy} obtained for the orientations of $\alpha = 30^o$ and $\alpha = 60^o$ for the same uniaxial stress σ_{xx} relate through

$$\varepsilon_{xx}^{60^o} = \varepsilon_{xx}^{30^o} \quad (185)$$
$$\gamma_{xy}^{60^o} = -\gamma_{xy}^{30^o} \quad (186)$$

which, again, let us explain the symmetric responses in the finite deformation context shown in Figures 8 and 9 of Ref. [59] (compare the cases $\alpha = 30^o$ and $\alpha = 60^o$ of each figure). Note that the reference configurations for $\alpha = 30^o$ and $\alpha = 60^o$ are different (i.e. they are not a reflection from each other). The symmetric responses are just a consequence of the plane strain condition, the incompressible behavior and the symmetry of the strain energy terms $\omega_{ij}(E_{ij}) = \omega_{ij}(-E_{ij})$ considered in that paper (as in the small strains case).

Another interesting view of this phenomenon may be obtained through the skew part of the Mandel stress tensor, used in Refs. [50, 63, 73] in the context of plasticity to account for the update of the principal material directions. This tensor, work-conjugate to spins and which may be interpreted as fictitious angular moments per unit volume (couple-stress), accounts for the lack of commutativity due to elastic anisotropy and is obtained from the elastic strains and stored energy function as

$$\boldsymbol{T}_w := \boldsymbol{E}\boldsymbol{T} - \boldsymbol{T}\boldsymbol{E} \quad (187)$$

For this particular case, using Eq. (176) and small strains

$$\boldsymbol{\sigma}_w := \boldsymbol{\varepsilon}\boldsymbol{\sigma} - \boldsymbol{\sigma}\boldsymbol{\varepsilon} = \begin{bmatrix} 0 & -\sigma_{w21} & 0 \\ \sigma_{w21} & 0 & 0 \\ 0 & 0 & 0 \end{bmatrix} \quad (188)$$
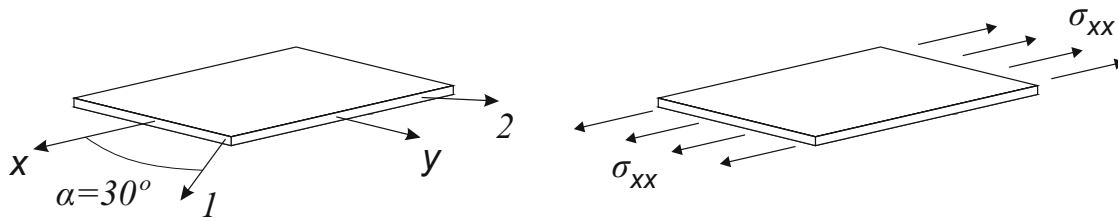
Fig. 14 Uniaxial test over an incompressible orthotropic specimen in which the preferred material axes $\{1, 2\}$ are not aligned with the test axes $\{x, y\}$.
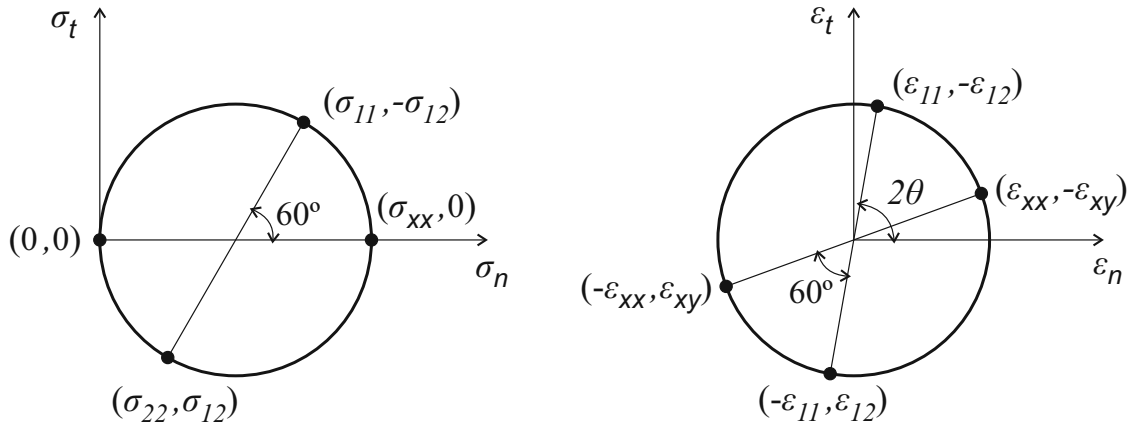

Fig. 15 Mohr's circles for stresses (left) and strains (right) associated to the uniaxial test under plane strain of Figure 14 with $\alpha = 30^o$. In the Mohr's circle of stresses we use $\sigma_{xy} = \sigma_{yy} = 0$ (boundary conditions). In the Mohr's circle of strains we use $\varepsilon_{yy} = -\varepsilon_{xx}$ (incompressibility). Subscript n means "normal" and subscript t means "tangential".

where

$$\sigma_{w21} = 2\varepsilon_{11}\varepsilon_{12}\left(\mu_{11} + \mu_{22} - 2\mu_{12}\right) \qquad (189)$$

Note that there is a change of sign if either $\mu_{11} + \mu_{22} - 2\mu_{12}$ (material dependent) changes sign or if $\varepsilon_{11}\varepsilon_{12}$ (load dependent) changes sign. Furthermore, for in-axis (axial) loading $\varepsilon_{12} = 0$ or pure shear loading $\varepsilon_{11} = \varepsilon_{22} = 0$, the tensor $\boldsymbol{\sigma}_w$ vanishes. Obviously for the isotropic case all μ_{ij} are coincident and $\boldsymbol{\sigma}_w$ also vanishes.

References

1. Cristensen RM (2003) Theory of Viscoelasticity. Dover.
2. Shaw MT, MacKnight WJ (2005) Introduction to Polymer Viscoelasticity. Wiley-Blackwell.
3. Argon AS (2013) The Physics of Deformation and Fracture of Polymers. Cambridge University Press.
4. Schapery RA, Sun CT (Eds) (2000) Time Dependent and Nonlinear Effects in Polymers and Composites. American Society for Testing and Materials (ASTM).
5. Gennisson JL, Deffieux T, Macé E, Montaldo G, Fink M, Tanter M (2010) Viscoelastic and anisotropic mechanical properties of in vivo muscle tissue assessed by supersonic shear imaging. Ultrasound Med Biol 36(5):789–801.
6. Schapery RA (2000) Nonlinear viscoelastic solids. Int J Sol Struct 37(1):359–366.
7. Truesdell C, Noll W (2004) The non-linear field theories of mechanics. Springer, Berlin, Heidelberg.
8. Rivlin RS (1965) Nonlinear viscoelastic solids. Siam Review 7(3):323–340.
9. Fung YC (1993) A First Course in Continuum Mechanics. Prentice-Hall.
10. Fung YC (1972) Stress-strain-history relations of soft tissues in simple elongation. Biomechanics: Its foundations and objectives 7:181–208.
11. Sauren AAHJ, Rousseau EPM (1983) A concise sensitivity analysis of the quasi-linear viscoelastic model proposed by Fung. J Biomech Engrg 105(1):92–95.
12. Rebouah M, Chagnon G (2014) Extension of classical viscoelastic models in large deformation to anisotropy and stress softening. Int J Non-Linear Mech 61:54–64.
13. Poon H, Ahmad MF (1998) A material point time integration procedure for anisotropic, thermo rheologically simple, viscoelastic solids. Comput Mech 21(3):236–242.
14. Drapaca CS, Sivaloganathan S, Tenti G (2007) Nonlinear constitutive laws in viscoelasticity. Math Mech Sol 12(5):475–501.
15. Simo JC, Hughes TJR (1998) Computational inelasticity. New York, Springer.
16. Holzapfel GA (2000) Nonlinear Solid Mechanics. A Continuum Approach For Engineering. Wiley, Chichester.

17. Peña JA, Martínez MA, Peña E (2011) A formulation to model the nonlinear viscoelastic properties of the vascular tissue. Acta Mech 217(1-2):63–74.

18. Peña E, Peña JA, Doblaré M (2008) On modelling nonlinear viscoelastic effects in ligaments. J Biomech 41(12):2659–2666.

19. Holzapfel GA (1996) On large strain viscoelasticity: continuum formulation and finite element applications to elastomeric structures. Int J Numer Methods Engrg 39(22):3903–3926.

20. Liefeith D, Kolling S (2007) An Anisotropic Material Model for Finite Rubber Viscoelasticity. LS-Dyna Anwenderforum, Frankenthal.

21. Haupt P (2002) Continuum Mechanics and Theory of Materials. Springer, Berlin, 2nd edition.

22. Bergström JS, Boyce MC (1998) Constitutive modeling of the large strain time-dependent behavior of elastomers. J Mech Phys Sol 46(5):931–954.

23. Le Tallec P, Rahier C, Kaiss A (1993) Three-dimensional incompressible viscoelasticity in large strains: Formulation and numerical approximation. Comput Methods Appl Mech Engrg 109:233–258.

24. Haupt P, Sedlan K (2001) Viscoplasticity of elastomeric materials: experimental facts and constitutive modelling. Arch Appl Mech 71:89–109.

25. Lion A (1996) A constitutive model for carbon black filled rubber: Experimental investigations and mathematical representation. Continuum Mechanics and Thermodynamics. Continuum Mech Therm 8(3)153–169.

26. Lion A (1998) Thixotropic behaviour of rubber under dynamic loading histories: Experiments and theory. J Mech Phys Sol 46(5):895–930.

27. Simo JC (1987) On a fully three-dimensional finite-strain viscoelastic damage model: formulation and computational aspects. Comput Methods Appl Mech Engrg 60(2):153–173.

28. Craiem D, Rojo FJ, Atienza JM, Armentano RL, Guinea GV (2008) Fractional-order viscoelasticity applied to describe uniaxial stress relaxation of human arteries. Phys Med Biol (53)4543-4554.

29. Kaliske M, Rothert H (1997) Formulation and implementation of three-dimensional viscoelasticity at small and finite strains. Comput Mech 19(3):228–239.

30. Gasser TC, Forsell C (2011) The numerical implementation of invariant-based viscoelastic formulations at finite strains. An anisotropic model for the passive myocardium. Comput Meth Appl Mech Engrg 200(49):3637–3645.

31. Reese S, Govindjee S (1998) A theory of finite viscoelasticity and numerical aspects. Int J Sol Struct 35(26):3455–3482.

32. Lubliner J (1985) A model of rubber viscoelasticity. Mech Res Commun 12(2):93–99.

33. Sidoroff F (1974) Un modèle viscoélastique non linéaire avec configuration intermédiaire. J Mécanique 13(4):679–713.

34. Lee EH (1969) Elastic-plastic deformation at finite strains. J Appl Mech 36(1):1–6.

35. Bilby BA, Bullough R, Smith E (1955) Continuous distributions of dislocations: a new application of the methods of non-Riemannian geometry. Proc R Soc Lond, Ser A, Math Phys Sci 231(1185):263–273.

36. Herrmann LR, Peterson FE (1968) A numerical procedure for viscoelastic stress analysis. In: Seventh Meeting of ICRPG Mechanical Behavior Working Group, Orlando, FL, CPIA Publication 177:60–69.

37. Taylor RL, Pister KS, Goudreau GL (1970) Thermomechanical analysis of viscoelastic solids. Int J Numer Methods Engrg 2(1):45–59.

38. Hartmann S (2002) Computation in finite-strain viscoelasticity: finite elements based on the interpretation as differential-algebraic equations. Comput Methods Appl Mech Engrg 191(13-14):1439–1470.

39. Eidel B, Kuhn C (2011) Order reduction in computational inelasticity: Why it happens and how to overcome it—The ODE-case of viscoelasticity. Int J Numer Methods Engrg 87(11):1046–1073.

40. Haslach Jr HW (2005) Nonlinear viscoelastic, thermodynamically consistent, models for biological soft tissue. Biomech Model Mechanobiol 3(3):172–189.

41. Pioletti DP, Rakotomanana LR, Benvenuti JF, Leyvraz PF (1998) Viscoelastic constitutive law in large deformations: application to human knee ligaments and tendons. J Biomech 31(8):753–757.

42. Merodio J, Goicolea JM (2007) On thermodynamically consistent constitutive equations for fiber-reinforced nonlinearly viscoelastic solids with application to biomechanics. Mech Res Commun 34(7):561–571.

43. Bonet J (2001) Large strain viscoelastic constitutive models. Int J Sol Struct 38(17):2953–2968.

44. Peric D, Dettmer W (2003) A computational model for generalized inelastic materials at finite strains combining elastic, viscoelastic and plastic material behaviour. Engrg Comput 20(5/6):768–787.

45. Nedjar B (2002) Frameworks for finite strain viscoelastic-plasticity based on multiplicative decompositions. Part I: Continuum formulations. Comput Methods Appl Mech Engrg 191(15):1541–1562.

46. Latorre M, Montáns FJ (2014) On the interpretation of the logarithmic strain tensor in an arbitrary system of representation. Int J Sol Struct 51(7):1507–1515.

47. Eterovic AL, Bathe KJ (1990) A hyperelastic-based large strain elasto-plastic constitutive formulation with combined isotropic-kinematic hardening using the logarithmic stress and strain measures. Int J Numer Methods Engrg 30(6):1099–1114.

48. Simo JC (1992) Algorithms for static and dynamic multiplicative plasticity that preserve the classical return mapping schemes of the infinitesimal theory. Comput Methods Appl Mech Engrg 99(1):61–112.

49. Caminero MA, Montáns FJ, Bathe KJ (2011) Modeling large strain anisotropic elasto-plasticity with logarithmic strain and stress measures. Comput Struct 89(11):826–843.

50. Montáns FJ, Benítez JM, Caminero MA (2012) A large strain anisotropic elastoplastic continuum theory for nonlinear kinematic hardening and texture evolution. Mech Res Commun 43:50–56.

51. Papadopoulos P, Lu J (2001) On the formulation and numerical solution of problems in anisotropic finite plasticity. Comput Meth Appl Mech Engrg 190(37):4889–4910.

52. Miehe C, Apel N, Lambrecht M (2002) Anisotropic additive plasticity in the logarithmic strain space: modular kinematic formulation and implementation based on incremental minimization principles for standard materials. Comput Meth Appl Mech Engrg 191(47):5383–5425.

53. Vogel F, Göktepe S, Steinmann P, Kuhl E (2014) Modeling and simulation of viscous electro-active polymers. Eur J Mech-A/Sol 48:112–128.

54. Holmes DW, Loughran JG (2010) Numerical aspects associated with the implementation of a finite strain, elasto-viscoelastic-viscoplastic constitutive theory in principal stretches. Int J Numer Methods Engrg 83(3):366-402.

55. Holzapfel GA, Gasser TC, Stadler M (2002) A structural model for the viscoelastic behavior of arterial walls: continuum formulation and finite element analysis. Eur J Mech-A/Sol 21(3):441–463.

56. Nguyen TD, Jones RE, Boyce BL (2007) Modeling the anisotropic finite-deformation viscoelastic behavior of soft fiber-reinforced composites. Int J Sol Struct 44(25):8366–8389.

57. Nedjar B (2007) An anisotropic viscoelastic fibre-matrix model at finite strains: continuum formulation and computational aspects. Comput Methods Appl Mech Engrg 196(9):1745–1756.

58. Latorre M, Montáns FJ (2013) Extension of the Sussman–Bathe spline-based hyperelastic model to incompressible transversely isotropic materials. Comput Struct 122:13–26.

59. Latorre M, Montáns FJ (2014) What-You-Prescribe-Is-What-You-Get orthotropic hyperelasticity. Comput Mech 53(6):1279–1298.

60. Latorre M, Montáns FJ (2015) Material-symmetries congruency in transversely isotropic and orthotropic hyperelastic materials. Eur J Mech-A/Sol 53:99–106.

61. Miñano M, Montáns FJ (2015) A new approach to modeling isotropic damage for Mullins effect in hyperelastic materials. Int J Sol Struct. In press, doi:10.1016/j.ijsolstr.2015.04.027.

62. Montáns FJ, Bathe KJ (2005) Computational issues in large strain elasto-plasticity: an algorithm for mixed hardening and plastic spin. Int J Numer Methods Engrg 63(2):159–196.

63. Montáns FJ, Bathe KJ (2007). Towards a model for large strain anisotropic elasto-plasticity. In: Computational Plasticity. Springer, Netherlands, pp 13–36.

64. Bathe KJ (2014) Finite Element Procedures. Second edition.

65. Weber G, Anand L (1990) Finite deformation constitutive equations and a time integration procedure for isotropic, hyperelastic-viscoplastic solids. Comput Methods Appl Mech Engrg 79(2):173–202.

66. Hartmann S, Quint KJ, Arnold M (2008) On plastic incompressibility within time-adaptive finite elements combined with projection techniques. Comput Methods Appl Mech Engrg 198:178-193.

67. Simo JC, Miehe C (1992) Associative coupled thermoplasticity at finite strains: Formulation, numerical analysis and implementation. Comput Methods Appl Mech Engrg 98(1):41-104.

68. Sansour C, Bocko J (2003) On the numerical implications of multiplicative inelasticity with an anisotropic elastic constitutive law. Int J Numer Methods Engrg 58(14):2131–2160.

69. Bischoff JE, Arruda EM, Grosh K (2004) A rheological network model for the continuum anisotropic and viscoelastic behavior of soft tissue. Biomech Model Mechanobiol 3(1):56–65.

70. Sussman T, Bathe KJ (2009) A Model of Incompressible Isotropic Hyperelastic Material Behavior using Spline Interpolations of Tension-Compression Test Data. Commun Num Meth Engrg 25:53–63.

71. Sussman T, Bathe KJ (1987) A finite element formulation for nonlinear incompressible elastic and inelastic analysis. Comput Struct 26:357–409.

72. Ogden RW (1997) Nonlinear Elastic Deformations. Dover, New York.

73. Kim DN, Montáns FJ, Bathe KJ (2009) Insight into a model for large strain anisotropic elasto-plasticity. Comput Mech 44(5):651-668.